Mário David Grosso Xavier

Licenciado em Ciências da Engenharia Física

Development of a system for adsorption measurements in the 77 – 500 K and 1 – 100 bar range

Dissertação para obtenção do Grau de Mestre em

Engenharia Física

Orientador: Prof. Dr. Grégoire Bonfait,
Professor Associado com Agregação,
Universidade Nova de Lisboa

Co-orientador: Dr. Daniel Martins,
Thermal Engineer,
Active Space Technologies

Júri

Presidente: Dr. Filipe Tiago de Oliveira
Arguente: Dr. Rui Ribeiro
Vogal: Dr. Grégoire Bonfait

FACULDADE DE CIÊNCIAS E TECNOLOGIA
UNIVERSIDADE NOVA DE LISBOA

Setembro, 2016

Development of a system
for adsorption measurements
in the 77 – 500 K and 1 – 100 bar range

Este documento foi gerado utilizando o processador (pdf)LaTeX, com base no template "unlthesis" [1] desenvolvido no Dep. Informática da FCT-NOVA [2]. [1] https://github.com/joaomlourenco/unlthesis [2] http://www.di.fct.unl.pt

Acknowledgements

First of all, I would like to thank my advisor, Prof. Grégoire Bonfait, for his guidance, commitment, for the opportunity provided to work in his laboratory and for helping me open the door to the field of Cryogenics. I must also extend these thanks to Daniel Martins, my co-advisor, who was always ready to help and contribute with valuable insight. It was an enriching experience to be a part of the project and the laboratory, both professionally and personally, and I can only hope to be a part of such a work dynamic in my future.

Also extremely helpful were the efforts and input of the members of the Laboratory of Adsorption Technology and Process Engineering at the Chemistry Department: Prof. José Paulo Mota, who clarified the system design equations at an initial stage and provided a lot of data to discuss and compare with, and Isabel Esteves and Rui Ribeiro, with whom our discussions about adsorption always allowed us to improve our system and learn something more.

I must also thank my colleagues who were present at the Cryogenics Laboratory during my work, Jorge Barreto, Miguel Baeta, and Patrícia Borges de Sousa, for their constant availability, help, and great company in both serious and less serious contexts.

Our work would have been made much more complicated without the abilities of the department's workshop and so thanks are extended to: João Faustino for the manufacturing of all the workshop-made pieces, and Eduardo Jobling for the brazing of both the gas manifold and the calibrated volume. Both are also thanked for their input.

To my girlfriend, Yen, for constantly pushing me to try harder, for listening to all my complaining, and for being an incredible inspiration. To my friends: Inês, my sincerest thanks for your infectious attitude, your company, and your constant encouragement; Francisco, for your friendship over the years, which will hopefully carry on even as we tread different paths in different places; Stella, for being a great friend all the way from cold Latvia and for the constant shared laughter. And finally, a huge shout-out to all the TeamSpeak and Praça de Espanha field regulars, with whom the videogames and football meant a necessary break once in a while. All of you made these sometimes stressful months much lighter in different, equally valuable ways.

Last and most definitely not least, to my family, my parents, my brother, my grandparents, I would like to express my strongest gratitude for all they have done over the course of theirs and my lives to help me achieve my goals. It would have been much rougher or perhaps impossible without them.

Abstract

Adsorption is a phenomenon present in various systems important to the field of cryogenics, having a great deal of relevance in the development of vibration-free coolers: these are crucial for the cooling of sensitive detectors, as they offer the possibility of using a sorption compressor, do not have moving parts and do not induce unwanted mechanical vibrations in the system, maintaining its sensibility and greatly minimizing wear due to use.

In the context of an ESA-funded project for the development of such a cooler, a study on adequate adsorption materials to use for the non-mechanical cryogenic compressor present in the final system was required. Considering this, a system for measurement of adsorption properties in the range of its operating pressures and temperatures was needed and, independently, also useful in future adsorption studies the laboratory decides to perform.

A brief historical and functional review of the adsorption phenomenon, its applications in cryogenics, and available and various methods for its measurement is made. The design and assembly of an adsorption measurement system, through the volumetric (also known as manometric) method, for temperatures in the 77 K to 500 K range and pressures up to 100 bar is detailed.

Proof pressure tests were made to validate the design of the vessel, with positive results. Other pre-measurement tests, such as heating and cooling assays, void and dead volume measurements, empty-vessel measurements, were all carried out with an intention to validate and characterize the developed system. A LabVIEW™ interface for the control and automatic acquisition of the system parameters was developed and tested throughout the whole process.

Results were taken using a sample of HKUST-1 (also known as $Cu_3(BTC)_2$ or Basolite™ C300) and compared against the results from another group, as well as a partner laboratory, from both their theoretical simulations and their commercial gravimetric system.

Keywords: adsorption, manometric method, cryogenics, vibration-free cooler

Resumo

A adsorção é um fenómeno utilizado em vários sistemas criogénicos, tendo grande relevância no desenvolvimento de *vibration-free coolers*: estes são cruciais para o arrefecimento de detectores sensíveis, pois oferecem a possibilidade de uso de um compressor de sorção, não têm partes móveis e não induzem vibrações mecânicas indesejadas no sistema, mantendo a sensibilidade e minimizando significativamente o desgaste proveniente do uso.

No contexto de um projecto financiado pela ESA para o desenvolvimento de um criorrefrigerador deste tipo, um estudo sobre materiais adsorventes adequados para o uso no compressor criogénico não-mecânico presente no sistema final foi necessário. Tendo isto em consideração, um sistema para medida de propriedades de adsorção na gama de pressões e temperaturas de funcionamento do compressor foi necessário, e também útil em futuros estudos de adsorção que o laboratório efectue.

Uma breve revisão histórica e funcional do fenómeno de adsorção, as suas aplicações na criogenia, e os disponíveis e variados métodos para a sua medição é efectuada. O projecto e montagem de um sistema de medidas de adsorção, através do método volumétrico (também conhecido como manométrico), para temperaturas entre 77 K e 500 K e pressões até 100 bar, é detalhado.

Testes de pressão preliminares foram efectuados para validar o desenho da célula, com resultados positivos. Outros testes pré-medição, tais como ensaios de aquecimento e arrefecimento, medições de volumes mortos, medições sem amostra, foram efectuados com a intenção de validar e caracterizar o sistema desenvolvido. Uma interface em LabVIEW^{TM} para controlo e aquisição automática dos parâmetros de todo o sistema foi desenvolvida e testada durante todo o processo.

Foram obtidos resultados usando uma amostra de HKUST-1 (também conhecido como $Cu_3(BTC)_2$ ou Basolite^{TM} C300) e comparados com os resultados de outro grupo e de um laboratório parceiro, tanto das suas simulações teóricas como do seu sistema gravimétrico comercial.

Palavras-chave: adsorção, método manométrico, criogenia, *vibration-free cooler*

Contents

List of Figures

List of Tables

Chapter 1

Introduction

One of the most important applications of space cryogenics is the cooling of infrared detectors in satellites with a wide array of purposes. The recent years saw, in Europe, the development of active coolers that are capable of providing significant cooling power at an operational temperature of around 50 K, to meet Earth infrared observation mission requirements. In the case of missions for space observation, such as, for example, the Infrared Space Interferometer Darwin, these detectors enable the precise search of other Earth-like worlds and analysis of their biological properties, as well as other astrophysical objects in a similar wavelength range [1]. It's within the optimization of these types of applications that the cooling of the detectors is of great importance. The most advantages are gathered by the so-called vibration-free coolers, cryocoolers that function without moving parts and so do not induce unwanted vibrations that negatively affect the infrared detection system.

In general, the compressor is the biggest source of vibrations in a cryocooler: a vibration-free cooler must then invariably use a vibration-free compressor. A possibility is the use of a sorption compressor, which, as opposed to mechanical compressors, works thermochemically: this difference is enough to eliminate or minimize unwanted vibrations during its functioning. One of the researched options for this application is the use of this type of compressor to enable a Joule-Thomson effect. Such a Joule-Thomson, vibration-free cryocooler is to be developed in a European Space Agency project. The objectives of this project are to design, manufacture and test what's called an *Elegant Breadboard Model* of a vibration-free cooler that can provide active cooling for temperatures in the range of 40 K to 80 K in order to answer the needs of potential future Earth observation infrared missions [2]. It is in this context that the study of adsorption materials to be used in the compressor was necessary.

This document will approach the work done in the design, development and testing of a system for adsorption measurements, with the intention to provide useful data on different adsorbent materials to aid the design and construction of an efficient adsorption compressor for a vibration-free Joule-Thomson cooler. This dissertation is split into five other chapters.

In chapter 2, the objectives of the work carried out and the project within which it is inserted are described. With an intention to lay the groundwork for an accurate understanding of the rest of the document, a general contextualization on the adsorption phenomenon and its different types, theories and applications in the field of cryogenics, with an emphasis on cryocoolers, is exposed, as well as a description of the sample used to validate the system.

In chapter 3, an overview of the various experimental methods for the measurement of adsorption properties, as well as a literature review pertaining to the most recent and pertinent adsorption results to the developed system are carried out.

In chapter 4, the most important aspects of the volumetric experimental setup that was developed are explored. After an initial summary of the layout and its key components, the dimensioning - from general design to volumes and thicknesses, considering the high pressures reached - is detailed for all these components: the adsorption vessel and the calibrated volume, as well as the cooling and heating system designed to cover the 77 K to 500 K range. The preparation of the vessel and the sample prior to mounting in the system is explained. A brief description of the LabVIEW^{TM} interface is also given, highlighting the automatic stabilization algorithm and the data acquisition system. Also included in this chapter are step-by-step descriptions of the experimental procedures, as well as an overview of the helium measurements of the system's volumes, which are fundamental for a later result analysis. A small section on the empty-vessel tests carried out with an aim to pre-validate the system elaborates on experiments made without an adsorbent sample, in an attempt to confirm the volumes present in the system by performing routine measurements.

In chapter 5, the results for adsorption of neon on HKUST-1 are presented, most notably in the form of adsorption isotherms, from which important data such as the isosteric curves, the heat of adsorption, and others can be derived. A quantitative error and correction analysis is performed to gauge possible sources of error or corrections and their influence. Our results are compared with those obtained by a commercial gravimetric system belonging to LATPE, a partner laboratory in the Chemistry Department, and with results for adsorption heat obtained by another group in 2013, as a means to validate our system.

Finally, in chapter 6, general considerations and conclusions taken from this work, as well as what to improve about the system in the near future.

The appendix includes all the drawings for important pieces that were engineered during the development of the system.

Chapter 2

Contextualization

2.1 Vibration-free cooler in the 40 – 80 K range

In 2014, the European Space Agency posted an *Announcement of Opportunity* detailing specified requirements for the "Development of a 40 K to 80 K vibration-free cooler".

This project was assigned to two companies, one of them being Active Space Technologies: a Portuguese company specialized in thermo-mechanical and electronics engineering for aerospace, defense, automotive, nuclear fusion and scientific applications. It is currently in progress in collaboration with the Cryogenics Laboratory and the Adsorption Technology Group (LATPE), both located in the Faculdade de Ciências e Tecnologia of the Universidade Nova de Lisboa (FCT-UNL). From it originated a Ph. D. thesis (J. Barreto, for the development of a functioning prototype), and two M. Sc. theses (adding to this one, M. Baeta, for the development of the nitrogen stage).

The cooler is projected to be of the Joule-Thomson type, split in two stages, one with nitrogen and another with neon (cooling power: 0.5 W at 80 K and 40 K, respectively). It's predicted to cover most of the 40 K to 80 K range. To avoid the vibration induced by the more common mechanical compressors used for gas compression, the compressor will be sorption-based. Advantages of the latter are discussed in a later section about cryocoolers.

The design and development of a system for adsorption measurements is then necessary for a more precise dimensioning of the adsorption compressor used in the project's cryocooler. For the first measurements taken on the system, the adsorbent sample was HKUST-1, a metal-organic framework that's attractive due to properties close to the desired ones and its commercial availability. The adsorbate gas used in the measurements was neon, the working fluid of the second stage of the cryocooler, due to, when compared to nitrogen, a lack of experimental data using HKUST-1 and its lower

tendency to adsorb. A brief description of the adsorbent is available in a later section.

2.2 Adsorption

Adhesion of any atoms, ions, or molecules provenient from a fluid to a surface is defined as adsorption. The process creates a layer of adsorbate on the adsorbent, at surface level.

This phenomenon can be explained by the existence of a negative surface energy, which is the driving force behind any surface phenomena: in a material, the surface atoms, which are not wholly surrounded by other adsorbent atoms, are more susceptible to binding with surrounding bodies due to this unbalanced and asymmetric configuration in comparison to the bulk atoms. The attracted particle (adsorbate) then fills in the pores on the surface of the solid (adsorbent) when this phenomenon occurs. It's worth noting that surface energy caused by atomic force imbalance is not the only factor for the characterization of adsorption properties, as the compatibility of pairs of adsorbents and adsorbates (usually called adsorption working pairs) is defined by several other properties [3], [4].

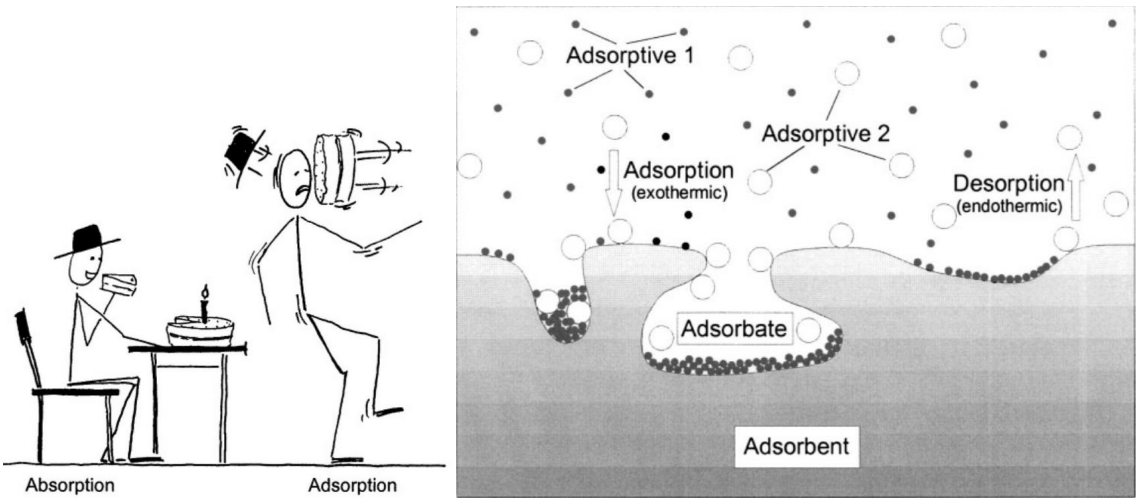

(a) (b)

Figure 2.1: In (a), the difference between absorption and adsorption in layman's terms. In (b), an illustration of adsorption with two adsorbates (or "adsorptives") and an adsorbent surface. Both taken from [5].

The term sorption encompasses both adsorption and absorption: differences between both lie in the fact that absorption involves permeation or dissolution of the absorbate in the absorbent, involving then the bulk of the material, as opposed to adsorption, which involves only the surface.

Adsorption is generally exothermic. One can intuitively explain this statement in several ways: for example, as explained above, adsorption leads to a lowering of the surface energy of the adsorbent, which necessarily means an exothermic process. Another

way to put it is to look at the equation for the Gibbs free energy, G, a thermodynamical potential that's minimized at chemical equilibrium at constant temperature and pressure: that means a diminishing G signifies a spontaneous, or favored, reaction. This potential was described by its eponym, J. W. Gibbs, as:

> ... the greatest amount of mechanical work which can be obtained from a given quantity of a certain substance in a given initial state, without increasing its total volume or allowing heat to pass to or from external bodies ... [6]

Its general definition is:

$$G(P,T) = H - TS \tag{2.1}$$

where G is the Gibbs free energy, P the pressure, T the temperature, H the enthalpy, and S the entropy, all pertaining to a **closed** system.

So, at constant temperature:

$$\Delta G = \Delta H - T\Delta S \tag{2.2}$$

Saying adsorption is exothermic is the same as saying the variation of enthalpy, ΔH, associated with adsorption is negative. Moreover, since the adsorption of a gas implies the restriction of its movement, an adsorption intuitively leads to a decrease in the entropy of the gas, and thus ΔS is negative. For the process to be spontaneous, or ΔG negative, seeing as ΔS is negative, ΔH must be necessarily negative enough to cancel out the positive $-T\Delta S$ term. Therefore, adsorption is generally exothermic, always for physisorption in particular but not necessarily for certain variants of chemisorption, however [7]. These two types of adsorption will be explained in subsection that follows.

2.2.1 Types of adsorption

Adsorption processes are mostly distinguished by the nature of the bonding processes involved, being usually characterized as chemical adsorption (or chemisorption) or physical adsorption (or physisorption). The distinction is basically the same as one between general chemical and physical interactions, and is sometimes difficult to make for some intermediate cases, such as strong hydrogen bonding [8] or weak charge transfers. This often complicates the modelling and analysis of a given system, since the methods for doing so vary depending on whether the phenomenon is chemical or physical. As will be elaborated below, the magnitude of the energies involved in each type of adsorption are very disparate, and so often times it is pertinent and helpful to calculate the adsorption enthalpy, for example, as to get a clearer picture [9].

2.2.1.1 Chemisorption

In this type of adsorption, the adsorbate reacts chemically with the adsorbent, becoming chemically bonded with it: this means that the chemical structure of the material's surface is altered, so generally only one layer – a monolayer – of a given adsorbate will form. It's a very selective process, depending heavily on the chemical nature of both adsorbent and adsorbate. The forces involved have a very short range, as characteristic of chemical bonds. Also to note is that this process is often irreversible, making it impossible to remove the adsorbed gas without altering the surface. Chemisorption has extremely high bond enthalpies: between 250 kJ/mol and 500 kJ/mol. In general, this very large enthalpy makes the use of this type of adsorption not viable for adsorption compressors. This is the main difference to physisorption.

2.2.1.2 Physisorption

Unlike chemisorption, physisorption occurs when the adsorbate remains on the adsorbent's surface due to weak, long-range Van der Waals or London forces. Since the binding energies involved are relatively weak (less than 20 kJ/mol), it's heavily influenced by temperature and pressure of the system: since physisorption is an exothermal process, low temperatures and high pressures contribute to adsorption, while high temperatures and low pressures lead to desorption. Due to the long-range of the forces and the non-chemical nature of these processes, it's possible to have multilayered adsorption as long as the forces involved allow it.

Within the context of this thesis, physisorption will be the sole focus, and so any mentions of adsorption from this point on refer to the physical, and not the chemical, type.

The exothermic property of physisorption mentioned earlier in this section is crucial to the functioning of an adsorption compressor and its quantification through the heat of adsorption will be done in the result analysis.

2.2.2 Theoretical formulations

To this date, at least 15 different isotherm models have been developed for adsorption studies. They have varying degrees of ideality and sophistication, as well as different cases in which they are applicable or not [10].

One of the simplest and most versatile models to date was derived by Langmuir, in 1918. This adsorbate-adsorbent system was treated by making several assumptions:

- The adsorbate behaves as an ideal, classical gas;
- The adsorbent surface is perfectly flat and homogeneous;
- The adsorbate becomes immobile after adsorbing;
- All the adsorption sites are equivalent;
- There are no interactions between adsorbed molecules.

The system is basically treated as a chemical system – though the reaction is not necessarily chemical – with reactions occurring for adsorption and desorption. The reagents are considered the free adsorbate molecules and the open adsorbent sites, and the products the adsorbent's occupied sites. Equalizing the chemical potentials of these two states, the central equation for the Langmuir model can be derived, which gives the percentage of filled adsorbent sites θ as a function of the gas pressure P_A:

$$\theta = \frac{KP_A}{1 + KP_A} \tag{2.3}$$

where K is a constant, dependent on reaction heat, particle mass and temperature. Equation 2.3 leads to the so-called Langmuir isotherms of adsorption, figure 2.2:

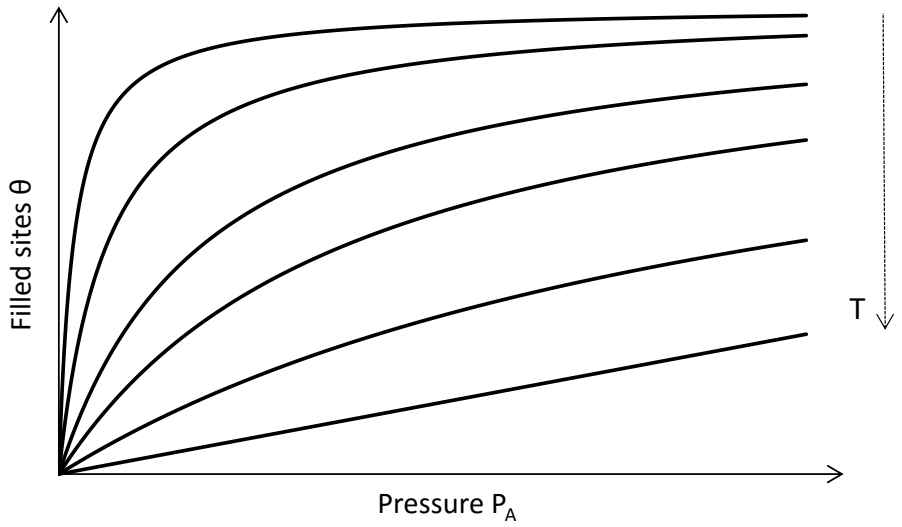

Figure 2.2: Example of typical Langmuir isotherms. For the same pressure, the highestθ signifies a lower temperature (as in, more adsorption at lower temperatures!).

It's interesting to note that the isotherms for high temperatures (which would be the lower adsorbed quantities θ in figure 2.2) exhibit a linear behavior with respect to pressure, while the isotherms for lower temperatures, where adsorption is more favored, exhibit much earlier saturation. This saturation reduces the effect of pressure at high pressures, as the adsorbent material's sites are then almost completely filled with the adsorbate gas. At low pressures, θ is proportional to P_A, which is called Henry's Law. This experimental law is confirmed by the limit of low pressure of the Langmuir model.

To understand the adsorption process, it's also important to know that it results in dynamic equilibrium: a coexistence of free molecules and adsorbed molecules, where both adsorption and desorption are constantly happening at the same rate. This can be described by equation 2.4, where the rates of adsorption and desorption are equaled:

$$K = \frac{K_a}{K_d} = \frac{[AB]}{[A][B]} \rightarrow K = \frac{\theta}{(1-\theta)P_A} \tag{2.4}$$

where $[A]$ is the quantity of free gas molecules (proportional to P_A), $[B]$ the quantity of unoccupied surface atoms (proportional to $1-\theta$) and $[AB]$ the quantity of adsorbed gas molecules (proportional to θ). K_a and K_d are the rates of reaction of adsorption and desorption, respectively. Rearranging equation 2.4, we obtain the former equation 2.3.

This model is widely used, both educationally and experimentally: it is applicable in most chemisorption phenomena as well as physisorption below a given saturation pressure, giving it versatility. Other models that take, for instance, multilayers (Brunauer-Emmett-Teller, or BET for short, often used to estimate adsorbent surface areas [11]), larger incidence of adsorption near already adsorbed molecules (Kisliuk [12]), and other factors into account, exist for applications where a higher degree of analysis is required.

Another important theoretical aspect is the calculation of the heat of adsorption. As already mentioned, adsorption leads to a dynamic equilibrium, and is an exothermal process, which means a molecule of gas transfers heat to its surroundings when it is adsorbed. By treating adsorption as a change of phase and the gas as ideal, we can apply the Clausius-Clapeyron equation to calculate the reaction heat (equation 2.5) [13]:

$$L = -R\frac{\delta(\ln(P))}{\delta\left(\frac{1}{T}\right)} \tag{2.5}$$

where L is the reaction heat, R the ideal gas constant, P the pressure and T the temperature of the system.

One important thing to keep in mind is that, in the specific case of adsorption, L is conventionally taken at isosteric conditions, meaning at constant adsorbed quantities θ. Essentially, the slope of an isosteric curve, which would be a horizontal line in figure 2.2, plotted with $\ln(P)$ and $\frac{1}{T}$, will give us the adsorption heat. This slope should be negative, as we concluded earlier from ΔH in equation 2.2.

This heat, as well as the isotherms, taken over the pressure range, are the two important parameters for the design of a working gas adsorption compressor.

2.2.3 HKUST-1 and other adsorbents

Currently used adsorbents can be split into several categories, depending on their typical surface area (which is always relatively large) and their intended and diverse applications: these can be industrial, medical, scientific, among others.

(a) (b)

Figure 2.3: In (a), activated carbon [14]. In (b), zeolite [15]. These are the two most used and commercialized types of adsorbents.

The most widely popular and commercialized adsorbent in cryogenics is activated carbon, a form of carbon processed in such a way that it has small, low-volume pores that give the material an enormous surface area: typically around 1000 m^2/g and as high as 3000 m^2/g [5]. The raw carbon is extracted from common carbonaceous materials such as nutshells, wood, and coal. The extraction is often called carbonization, and is performed through pyrolisis (thermochemical decomposition of organic materials in an inert environment) in the temperature range from 600 ºC to 900 ºC. The carbon product's surface area is then enhanced through physical or chemical means, called activation. In the physical case, this means exposure to an oxidizing atmosphere at very high temperatures (600 ºC to 1200 ºC), while in the chemical case, it means impregnation of the raw material with certain strong chemicals. A convenient property of activated carbon is that it has a great variety of heavily researched methods for its regeneration, such as ultrasound [16], electrochemical [17] and microwave-assisted [18] methods, not necessarily requiring high temperatures to desorb all the gas it holds.

Other very common commercialized adsorbents are zeolites, which are microporous, aluminosilicate minerals that, due to their very regular molecular-sized pore structure, have the ability to only allow adsorption to molecules smaller than a given size. This ability puts this material in the family of solids known as molecular sieves and makes them very attractive for molecular separation and trapping. The typical surface areas are around 500 m^2/g.

HKUST-1, the material used to make measurements with the developed system, is an adsorbent categorized as a metal-organic framework and available under the commercial name Basolite^{TM} C300, manufactured by Sigma Aldrich (Germany). Its chemical denomination is $Cu_3(BTC)_2$. Table 2.1 summarizes and highlights some interesting properties as an adsorbent of this commercialized variant of HKUST-1.

Table 2.1: Physical properties of Basolite^{TM} C300, adapted from [19].

Property	HKUST-1
Activation conditions	423 K under vacuum (10 h)
Molecular weight	605 g/mol
Particle size	16 µm
Bulk density	350 kg/m^3
BET surface area	1500 to 2100 m^2/g

This material was one of options for the project's adsorption compressors due to its capacity in adsorbing both nitrogen and neon better than activated carbon. As already mentioned in section 2.1, adsorbing neon is conventionally less favorable: this is due to its little or no ability to react when compared to non-noble gases. It was tested on due to its quick availability when compared to the other analyzed metal-organic frameworks, that were both not commercial and not simple to synthesize.

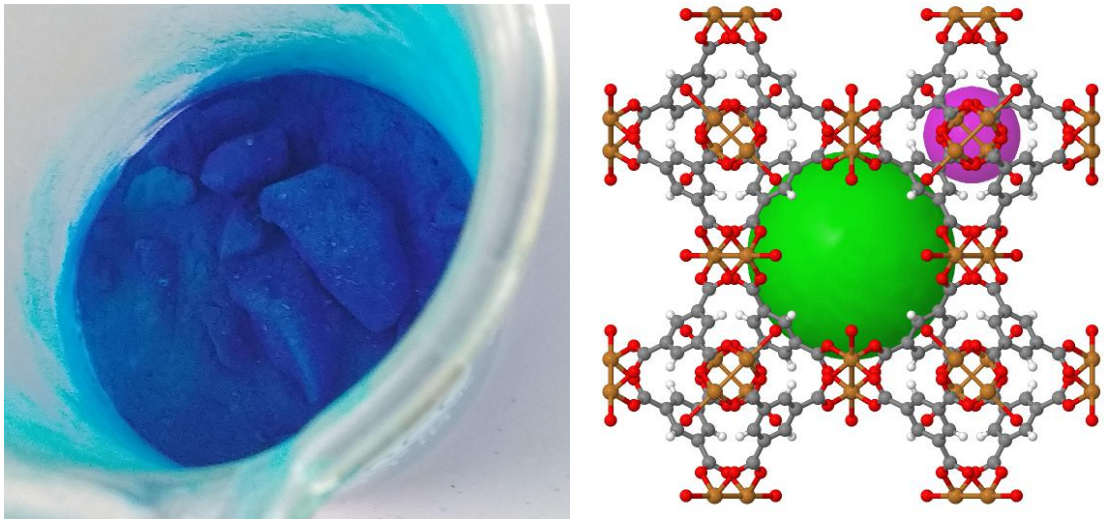

(a) (b)

Figure 2.4: In (a), HKUST-1 in its powder form, as it is provided commercially. Note the darker and lighter hues of blue, corresponding to different states of oxidation (reversible). In (b), the molecular framework of HKUST-1, with spheres representing the pore sizes within it that can be used for gas storage. The green sphere has a diameter of approximately 10 Å. [20]

These conclusions were attained through simulations done by Prof. J. P. Mota, from LATPE, who analyzed several possible adsorbent samples for the working gases [21].

2.2.4 Applications in cryogenics

2.2.4.1 Cryocoolers

Adsorption is usually not the concept directly behind any type of cooling. However, it can be used in several types of cooling cycles through sorption-based compressors [22], where the pressure cycles are generated through heating and cooling cycles of adsorbent-filled containers, generally called adsorption vessels. These compressors have the advantage that they do not have any moving parts, which severely minimizes their vibrations and wear due to use: this makes them attractive for a great variety of applications, where lifetime and the lowest possible level of vibrations are an important factor [23], such as in the project in which this thesis is inserted.

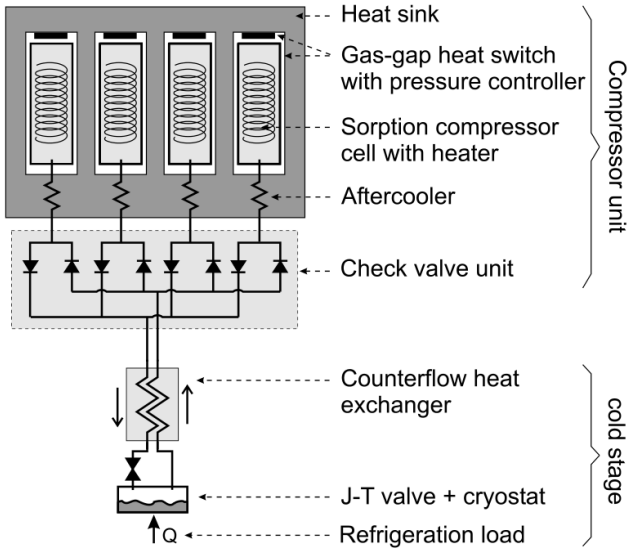

Figure 2.5: Schematic of a generic Joule-Thomson cryocooler using adsorption compressors [1] [a].

[a] Reprinted from Cryogenics, Vol. 42, nr. 2, J. F. Burger et al, Vibration-free 5 K sorption cooler for ESA's Darwin mission, pp. 97–108, Copyright 2002, with permission from Elsevier.

For example, within the scope of the already mentioned project, the functioning of a Joule-Thomson sorption cooler (figure 2.2.4.1) will be detailed to illustrate the importance of the compressor and its control.

As the name suggests, a Joule-Thomson cryocooler takes advantage of the Joule-Thomson effect to cool a working fluid. This effect, also known as a throttling process, consists of the temperature change of a real (as opposed to ideal) fluid when forced through a thermally insulated restriction, which results in a (Joule-Thomson) expansion. This results in cooling or heating depending on the fluid's thermodynamic properties. The thermally insulated restriction is considered a small enough channel or orifice to force a large pressure change. Since no heat is exchanged with the surroundings, it can be proven that this process is isenthalpic ($\Delta H = 0$).

The equation that determines the Joule-Thomson coefficient that rules over this phenomenon is as follows:

$$\mu_{JT} = \left(\frac{\partial T}{\partial P}\right)_H = \frac{V}{C_p}(\alpha T - 1) \tag{2.6}$$

In which μ_{JT} is the Joule-Thomson coefficient, T, P and H the gas temperature, pressure and enthalpy, respectively, V the volume, C_p the heat capacity at constant pressure, and α the thermal dilation coefficient of the fluid. As it represents the variation of temperature with pressure of an isenthalpic process, a positive Joule-Thomson coefficient yields a cooling with expansion: the pressure decreases, and thus the temperature must decrease. A negative Joule-Thomson coefficient results in heating: the pressure decreases, and thus the temperature must increase. The variation of this coefficient's signal leads to the so-called inversion temperature, T_{inv}: above this temperature, the coefficient is always negative, while below it, it is positive. Hydrogen, helium and neon have inversion temperatures lower than 300 K at atmospheric pressure, requiring then some pre-cooling in order to take advantage of the Joule-Thomson effect.

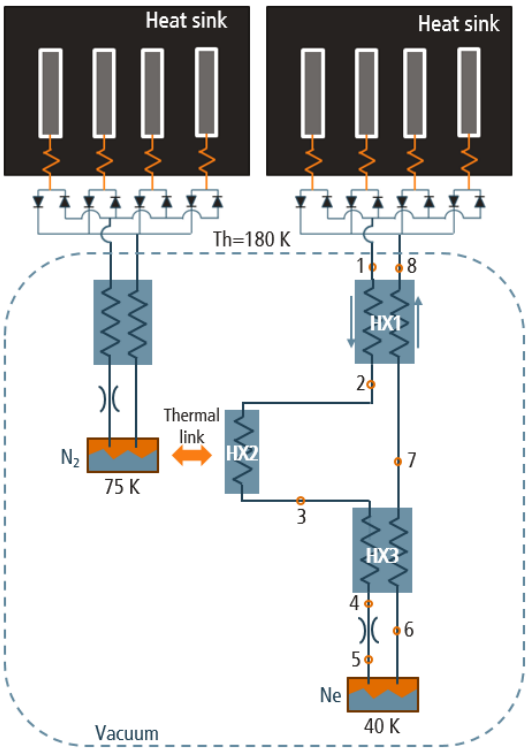

Figure 2.6: Diagram of the project's two-stage cryocooler. Adapted from [24].

This pre-cooling could, in theory, be done with the two-stage configuration represented in figure 2.6: the nitrogen stage could pre-cool the neon stage through a thermal link so that neon could cool through a Joule-Thomson expansion. In the project's case, however, it's purely to enhance the efficiency of the cycle. Heat exchangers are

constant presences in these cryocoolers to facilitate pre-cooling and increase the cooler efficiency, as well as any other heat transfers present in the system. Despite being a part of the project, these elements will not be discussed in detail within this thesis, as they are not present in the developed adsorption measurement system (M. Baeta, M. Sc. thesis).

Sorption compressors are cyclical systems in which the adsorption vessels alternate between adsorption and desorption (respectively, lowering and raising pressure) through the variation of temperature. As already mentioned in the description of physisorption, temperature has a strong influence in these phenomena. However, to avoid strong fluctuations of gas flow, which are harmful to the temperature stability of the Joule-Thomson cycle, one needs at least four vessels, functioning out-of-phase with each other, with adequate check valves [1].

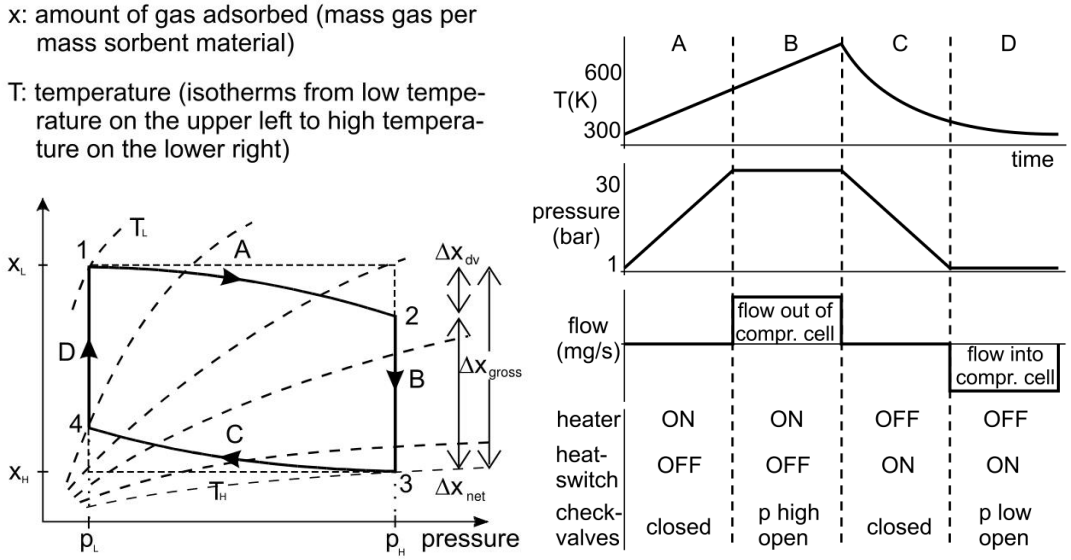

Figure 2.7: Working cycle of a 5 K Joule-Thomson cryocooler's adsorption compressor, taken from [1] [a]. In (a), the cycle drawn over generic adsorption isotherms. In (b), the variation of the several system parameters over the cycle.

[a] Reprinted from Cryogenics, Vol. 42, nr. 2, J. F. Burger et al, Vibration-free 5 K sorption cooler for ESA's Darwin mission, pp. 97–108, Copyright 2002, with permission from Elsevier.

A typical compressor cycle is shown in figure 2.2.4.1 and corresponds to the cryocooler schematized in figure 2.2.4.1. In a first phase, A, a vessel is warmed up, which results in desorption. This compresses the gas, raising the pressure, which upon reaching a certain value (in the example, 30 bar) opens the high pressure check valve (see figure 2.2.4.1), resulting in a flow of desorbed gas exiting the vessel towards the expansion valve in a second phase, B. In a third phase, C, the heating is closed and the vessel connected through a heat switch to a cold source (heat sink), leading to a cooling of the vessel and consequent adsorption, which decompresses the gas, lowering the pressure: this closes the high pressure check valve. As the pressure reaches the low pressure check valve

limit (in the example, 1 bar), the valve opens, which establishes a flow of adsorbing gas entering the vessel from the expansion valve in a fourth phase, D. Two pairs of vessels operating in opposed phase manage to damp the flow fluctuations inherent to this cycle.

2.2.4.2 Cryopumps

In the field of vacuum technology, cryopumps are a constant presence in high and ultra-high vacuum systems. They are clean, fast vacuum pumps that work through removal of gases and vapors through condensation and adsorption on cold surfaces.

Condensation of particles on the cold surface happens when the vapor pressure of a given gas at the given cold temperature is so low that the condensed phase forms, effectively removing the gas particle from the system's volume. Unfortunately, the condensation of neon, hydrogen and helium is impossible with most cryopumps, because the vapor pressure of the former two at 20 K (the temperature limit for a relatively simple and usual cryocooler) is considerably high and the liquid phase for helium appears only below 5 K. The adsorption of these gases, however, doesn't suffer from this temperature limitation, which makes it a very good complement to the condensation process, making this a relatively effective pump for all types of gases, yet with some limitations for helium.

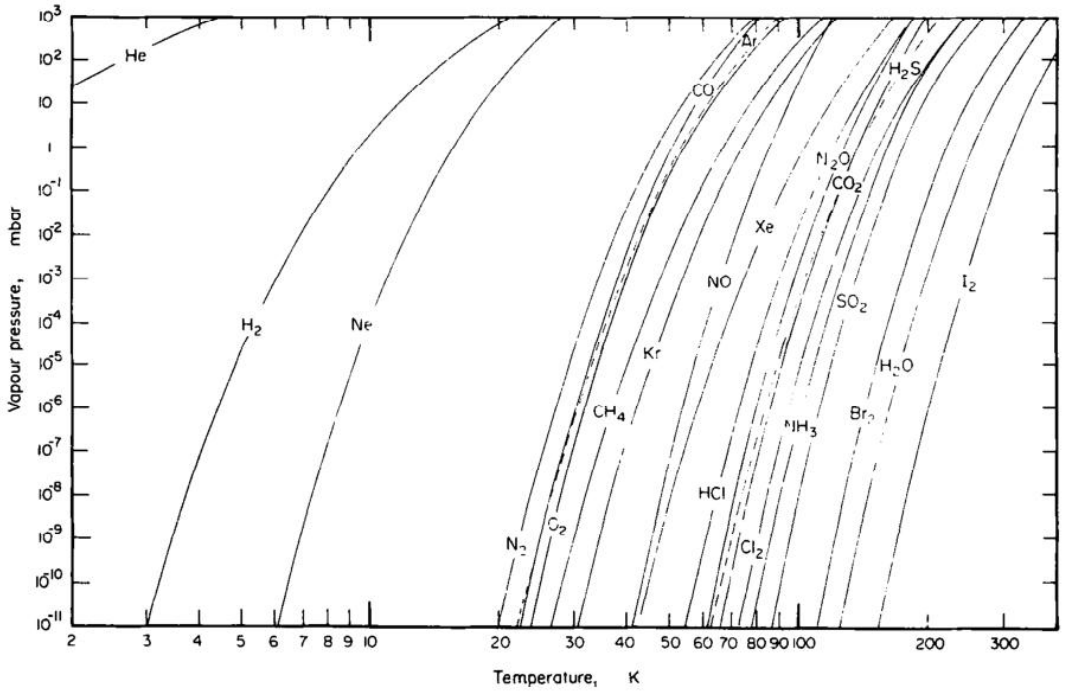

Figure 2.8: Vapour pressure vs. temperature for common pumped gases [25] [a]

[a] Reprinted from Vacuum, Vol. 30, nr. 30, P. D. Bentley, The modern cryopump, pp. 145–158, Copyright 1980, with permission from Elsevier.

Let us keep in mind that these phenomena of condensation and adsorption cannot

occur for an infinite number of particles, or an infinite amount of time, without "cleaning out" the system: this process, called regeneration, involves the warming of the cryopump to a high temperature, allowing the trapped gases and vapours to go back to a gaseous state, being then removed from the system by the appropriate pumping system.

2.2.4.3 Heat switches

As their name suggests, heat switches are devices with the capability to switch as needed between a high and a low thermal conductance state. Many types of heat-switches exist, but the gas gap heat switch is where adsorption plays a major role. It's nowadays in use for some satellites where cryogenics take part due to its peculiar, advantageous characteristics in space conditions: it is both compact and without moving parts when actuated by a cryopump.

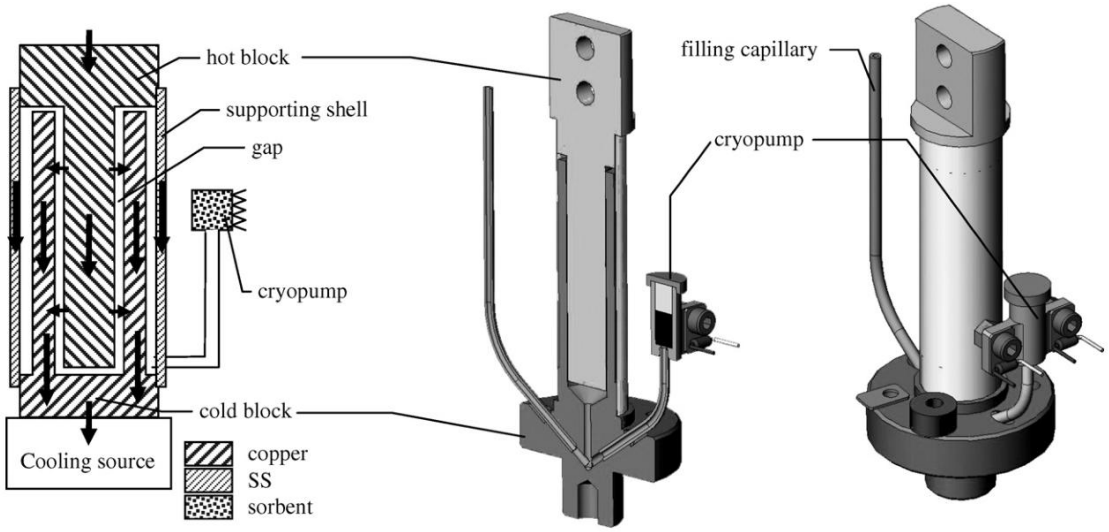

Figure 2.9: Structure of a gas gap heat switch, adapted from [26] [a].

[a] Reprinted from Cryogenics, Vol. 48, nr. 1, I. Catarino et al, Neon gas-gap heat switch, pp. 17–25, Copyright 2008, with permission from Elsevier.

The prototype in figure 2.2.4.3 consists of two cylindrical copper blocks, separated by a 100 micron gap and mechanically supported by a thin stainless steel shell. A miniature cryogenic adsorption pump is temperature regulated: when the temperature is lowered, adsorption is favored and thus a vacuum is created between the two copper blocks. If the vacuum is high enough to induce a molecular regime (where the mean free path λ is much larger than the gap Δ), the thermal resistance R of the gap is inversely proportional to the pressure, which induces a state of very low thermal conductance. As one heats up the cryopump, desorption occurs, which breaks the vacuum: this leads to a lower thermal resistance due to higher pressure. In reality, the change of regime to viscous (where λ is much smaller than Δ) makes the thermal resistance become independent of pressure and so a high thermal conductance state is reached [26].

Chapter 3

State of the art

3.1 Experimental methods

To dimension a system, the characteristic adsorption isotherms (for instance, figure 2.2.4.1, bottom left, $X(T,P)$) must be known. It is on this topic that a small overview of adsorption measurement methods currently in use is done in this chapter, with historic contextualization and current developments in each of them. The overview on experimental methods is based heavily on [5].

3.1.1 Volumetric method

The volumetric (or manometric) method is considered the pioneer of adsorption measurements, with early experiments situated in the late 1700s up to the early 1900s. A prototype of what is the current typical setup was developed and established in the 1940s.

It consists on the principle that if a given quantity of gas is well known, it can be expanded into a pre-evacuated vessel with an adsorbent sample in it. As the expansion is carried out, the quantity of gas is split into partially adsorbed on the adsorbent and partially remaining in the proximity of the adsorbent in a gaseous state. Through conservation of mass and knowledge of the void volume (the volume in which the adsorbate gas can enter), the amount of gas being adsorbed can be calculated.

The measurement is conventionally done through the variation of the equilibrium pressure from the initial state, where a calibrated, well-known volume is filled with a given quantity of gas, to the final state, where the initial quantity of gas has expanded to an adsorption vessel containing an adsorbent material, and has partially adsorbed. One can immediately relate a change in pressure inside the two known volumes to a change in quantity of gas through an equation of state, usually the ideal gas equation, depending

on the particularities of the system. This change in gas quantity is the adsorbed quantity, as adsorbed particles don't contribute to gas pressure. Because the pressure measurement is the key of this determination, the name "manometric" is also conventionally used.

A typical experimental setup for this method is displayed in figure 3.1.

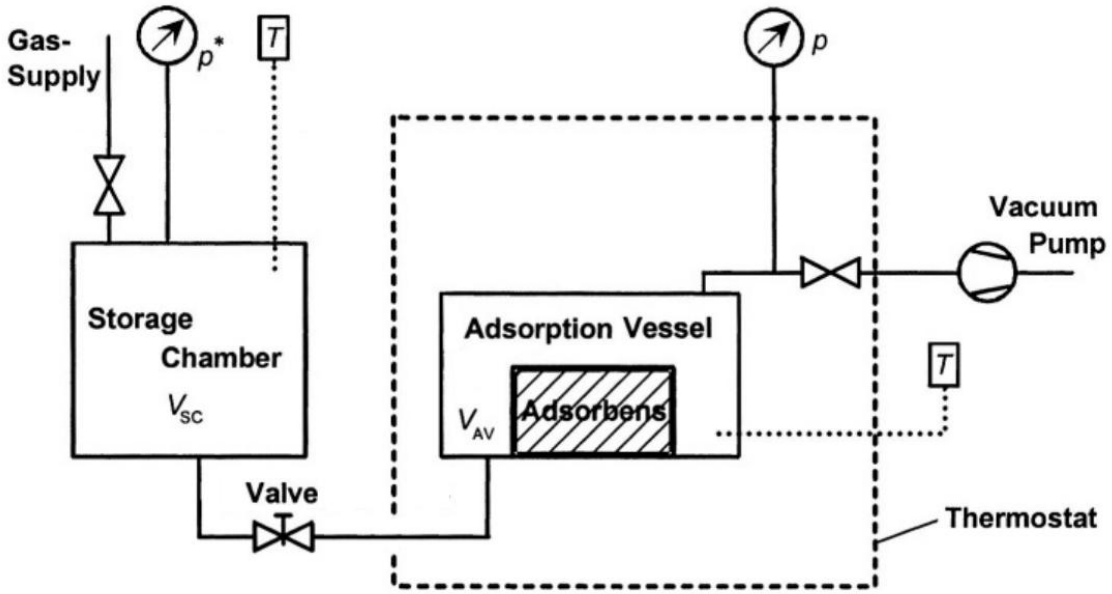

Figure 3.1: Typical volumetric method measurement system, adapted from [5].

What's remarkable about this method is that it is in many ways simple and effective, as a measurement is done by opening a valve and measuring a final pressure in the system, which makes it convenient for the programming of an acquisition system. It also gives the user complete temperature control, as the sample can be mounted on a cold source without any hindrances. The disadvantages are that there should be enough adsorbent in the vessel, usually several grams, for a pressure variation to be discernible — this can be an issue when the quantity of sample available is low or when it is relatively expensive — and that the pre-determination of the void volumes and the calibrated volume should be as accurate as possible to obtain accurate measurements, which implies that the existence of unknown volumes must be minimized. There has to be a compromise between the calibrated volume, the vessel volume (and so the adsorbent material quantity) and the amount of gas initially in the system for the variation in pressure to be measurable. This is the method for which the final system was dimensioned and the specifics of its application will be further detailed in chapter 4.

3.1.2 Gravimetric

The physical principle behind gravimetry is millennia old, dating back to biblical times, when the comparison of masses through weighing in the Earth's gravity field was first done, having not been applied to adsorption until much later due to technological

restraints. The gravimetric method as it is applied today, concerning adsorption phenomena of gases on solids, is then relatively recent, from the second half of the 1900s.

The method is based on the fact that an adsorbent on which an adsorbate accumulates undergoes a variation in mass, equal to the mass of the adsorbed gas. Thanks to noticeable improvements of weighing techniques and microbalance quality, this method is nowadays very sensitive. Within the gravimetric methods, different variants can be distinguished, dependent on the type of balance used, whether the balance is a single or double beam type, and the temperature region exploited.

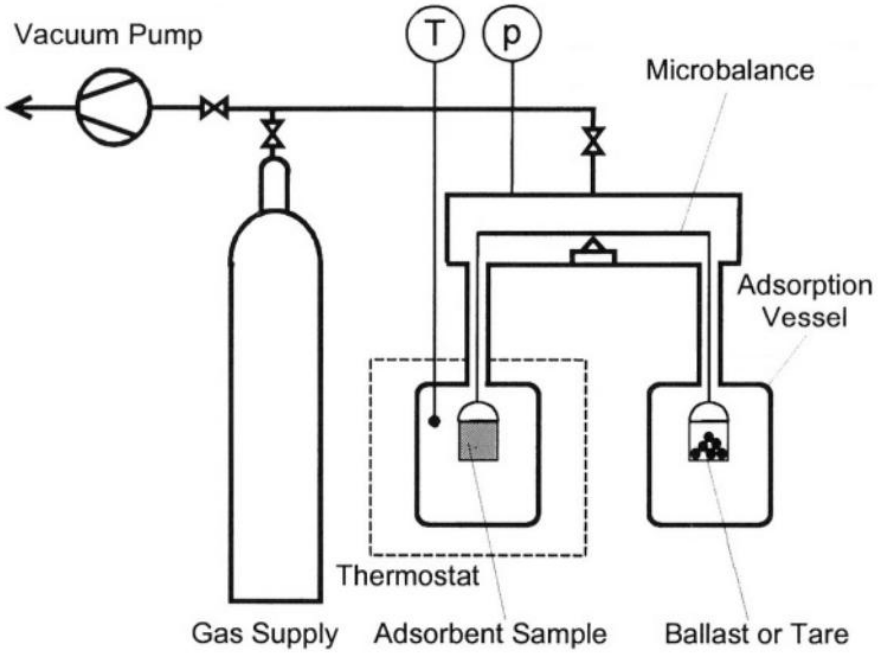

Figure 3.2: Typical gravimetric method measurement system, adapted from [5].

Though there are no corrections for void volumes to be done, the fact that the sample is usually immersed in the adsorbate gas requires a correction for the apparent weight it takes on due to buoyancy (Archimedes principle), depending on the gas density in the sample chamber. Another disadvantage is the cost and sophistication of such a system, when compared to its manometric counterpart. There is also the problem that temperature control can be more complicated due to the sample being on a balance, which makes cooling only possible through cryogenic liquids, with the disadvantages that entails when opposed to a connection to a cryocooler's cold finger. There is also no longer the issue of the gas adsorbing on the wall, since the measurements are done purely on the adsorbent. Advantages include a much greater sensibility due to greatly reduced elements of error, the relatively little amount of adsorbent material required, and that a great insight into the kinetics of adsorption can be obtained with sophisticated, high-speed acquisition microbalances.

3.1.3 Others

Several other recent methods exist besides the two aforementioned ones, with varying levels of popularity and divulgation. Again, most of this subsection is mainly based on [5].

Volumetric-gravimetric systems are systems in which the two previously described methods are applied simultaneously, in order to both conjugate the advantages of the two and to be able to determine coadsorption equilibria of gas mixtures without requiring a chromatograph or mass spectrometer. They are specially applied to industrial process control and design.

The oscillometric method, or oscillometry, consists of a pendulum or a freely floating rotator in slow rotational oscillation, coated with adsorbent material, where the damping of the movement of the chosen structure in a surrounding adsorbate is due to both the adsorption phenomenon and the friction with the gas. Measurements can be made optically, to gauge the movement properties of the structure in use. The chamber is in a thermostatic bath, which brings the same disadvantage as the gravimetric method: lack of good sample temperature control.

The impedance spectroscopy method relies on the basis that, if a static or alternating electric field is applied to a weakly electrical conducting or dielectric material — which encompasses most activated carbons, materials typically used for adsorption studies — the electrons and nuclei of the components are shifted in opposite directions to each other. This induces dipole moments in the material, which are measurable through the capacitance C or impedance Z of capacitors filled with the material in question. One gets C(f) or Z(f) curves, where f is the frequency of the applied electric field, which are characteristic for the adsorbent material in vacuum and for adsorbent/adsorbate systems. Through pre-calibration with the aid of other methods, such as manometric or gravimetric, one can obtain a curve that relates capacitance or impedance to quantity of adsorbed gas. This makes impedance spectroscopy also highly automatable, sharing the rest of the advantages and disadvantages of gravimetry.

3.2 Literature review of adsorption data on HKUST-1

In this section, there is a succinct review of published work done by other groups that is pertinent to our goals. This means, essentially, volumetric measurements in high temperature and pressure conditions compared to the usual range, performed in HKUST-1.

First of all, as mentioned in [27], from 1984, a hefty amount of experimental data for low-pressure cryogenic adsorption exists due to applications of adsorbents in cryo-pumping and low-pressure gas removal processes. Due to HKUST-1 and other types of metal-organic frameworks having not yet been developed at that time, the sample used for this work was activated carbon, which we've already concluded to have relatively

lesser performances for neon and nitrogen adsorption. Chan, C.K. *et al*, however, shared our goal of application in adsorption compressors, and thus covered a large range of temperatures and pressures (77 K to 400 K, 1 atm to 80 atm).

More recently, in 2011, Moellmer, J. *et al* also treated high-pressure adsorption (up to 500 bar), this time for HKUST-1, using however a much smaller temperature range (273 K to 343 K) [28]. These were, at the time, reported to be the first high-pressure (over200 bar) measurements done on this sample. As explained in the paper's introduction and to further explain the lack of extensive literature on this topic, most of HKUST-1's current applications lie in the lower pressure range: at the time of publishing and to the best of their knowledge, the only other literature found for high pressure adsorption measurements on HKUST-1 was a volumetric and gravimetric analysis of methane adsorption in a group of metal-organic frameworks [29], going up to 200 bar.

In 2013, an interesting study on noble gas adsorption in HKUST-1, experimental and computational [30], provides us with values for adsorption heats for neon adsorption, with which we'll compare our results in addition to the ones simulated and obtained by LATPE in subsection 5.3.3.

In 2014, Raganati, F. *et al* analyzed CO_2 capture in HKUST-1 in a sound assisted bed [31], having in parallel confirmed several physical properties. The most interesting in our perspective was a thermogravimetric analysis which gives us a reasonable profile of the behavior of the material with temperature, giving us an absolute maximum temperature limit of circa 350 ºC (see figure 3.2). This motivated us to perform a thermogravimetric analysis to confirm their results, since the temperature maximum is of great importance to our measurements and the soldered sealing of our vessel (see section 4.3).

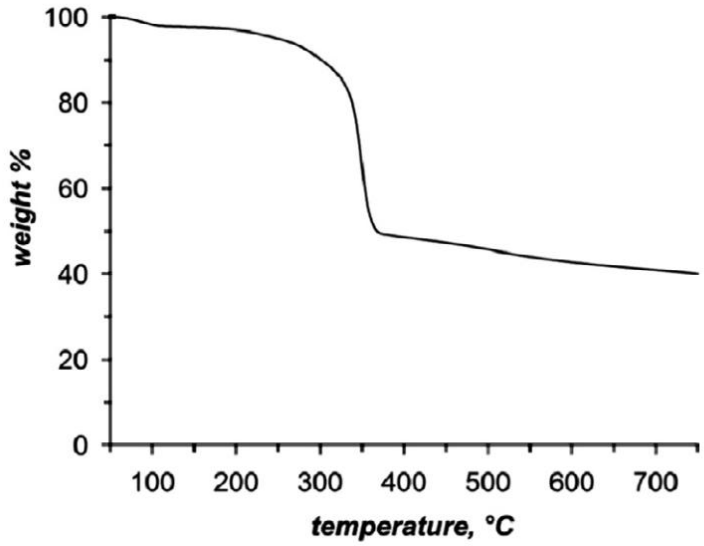

Figure 3.3: Thermogravimetric analysis of HKUST-1 in an N_2 environment. Adapted from [31] [a].

[a] Reprinted from Chemical Engineering Journal, Vol. 239, F. Raganati et al, CO_2 capture performance of HKUST-1 in a sound assisted fluidized bed, pp. 75–86, Copyright 2014, with permission from Elsevier.

As already mentioned, the literature for this neon adsorption on HKUST-1 paired with this range of temperatures and pressures was, to the best of our knowledge and at the time of writing, not possible to be found. As such, our results, presented in chapter 5, expand the usual temperature range of neon on HKUST-1 adsorption, and in specific providing data for applications in the more extreme temperature and pressure range applications, such as adsorption compressors, as in this project and the already mentioned work [27].

CHAPTER 4

EXPERIMENTAL SETUP

4.1 System summary and the volumetric method

As mentioned in the former chapter, the volumetric method was chosen for our measurements. A diagram summarizing the developed system is displayed in figure 4.1.

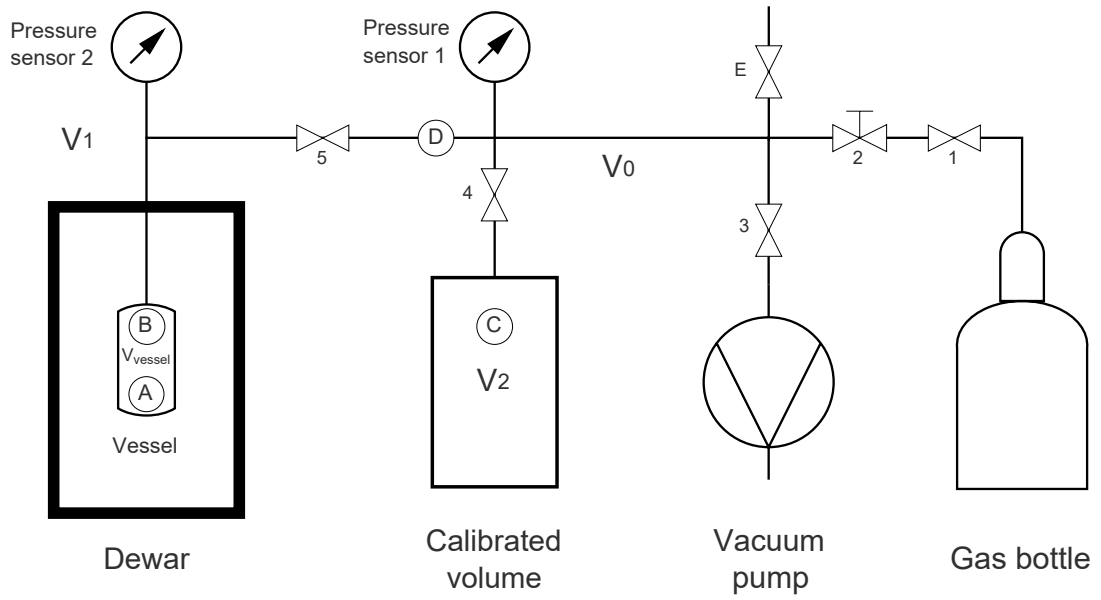

Figure 4.1: Gas system of the built system. The Pt100 thermometer locations are given by letters A through D.

The system consists of an adsorption vessel V_{vessel}, thermally protected inside a liquid nitrogen dewar and equipped with a system for temperature control which will be detailed in section 4.5. The vessel contains a certain quantity of adsorbent, and is connected through a capillary to a gas manifold containing two pressure sensors and a

calibrated volume V_2, used as a buffer and for the initial gas quantity determination. Also connected to the manifold are the gas bottle, from which the sample adsorbate is provided, and a rotary vacuum pump, for cleaning out the whole system.

Valves 1 and 2 are used for the supply of gas, 1 being the adjustable supply, so we can establish a given initial pressure, and 2 a quarter-turn valve. Valve 3 is the pumping valve, and valve E the escape valve, opened in the case of a non-pumpable pressure excess in the system. Valves 4 and 5 constitute the interface between the calibrated volume and the adsorption vessel. Operation of this manifold will be further discussed in section 4.6.

The expression that rules over the system is the mass balance at a given equilibrium pressure and system temperatures:

$$N_{vessel}(P, T_{A/B}) = N_{total} - N_{V_2}(P, T_C) - N_{V_1}(P, T_D) - N_{V_0}(P, T_D) \tag{4.1}$$

where N_{total} is the total number of molecules in the system, N_{vessel} the total number of molecules in the vessel (adsorbed or in a gaseous state), N_{V_x} $(x = 0, 1, 2)$ the number of molecules in the several non-vessel volumes in the system, for a system pressure P, and the several system temperatures T_X $(X = A, B, C, D)$, as per the designations of the thermometers in figure 4.1.

N_{vessel} can then be used to determine the adsorbed quantity in the vessel, knowing some other parameters that are explained below:

$$N_{vessel}(P, T_{A/B}) = V_{vessel}\left(\epsilon\rho_g(P, T_{A/B}) + (1-\epsilon)\rho_p q^*(P, T_{A/B})\right) \tag{4.2}$$

where V_{vessel} is the vessel's volume, ϵ the packing factor, ρ_g the gas density at the vessel's temperature and pressure, ρ_p the particle density, and q^* the specific adsorbed quantity.

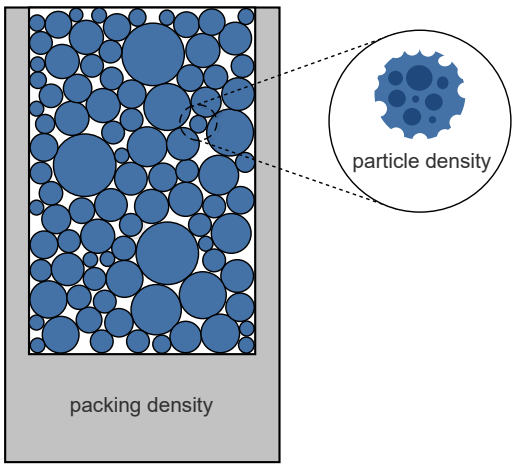

Figure 4.2: The densities in the system.

There are two densities referring to the material in this model, so a description of each is needed, with the help of figure 4.2:

ρ_p, the so-called particle density, is the mass density of a single particle (its weight divided by its apparent volume) and so it takes into account the porosity that adsorbent materials have (see in the figure, zoomed in) and is often a material-specific constant.

ρ_b, the so-called packing density, is calculated by dividing the quantity of adsorbent by the volume in which it is packed (equation 4.3). This density then takes into account not only the porosity

of the particle, but also the inter-particle space (figure 4.2) that an imperfect packing inevitably has.

$$\rho_b = \frac{m_{adsorbent}}{V_{vessel}} \tag{4.3}$$

The packing factor, ϵ, tells us what fraction of the vessel corresponds to inter-particle space, which is not filled by adsorbent. In essence, a perfect packing ($\epsilon = 0$) would yield a packing density equal to the particle density, as no interparticle space would exist:

$$\epsilon = 1 - \frac{\rho_b}{\rho_p} \tag{4.4}$$

We can now look at equation 4.2 and understand the two terms: the first, multiplied by ϵ, refers to the portion of the vessel not filled by adsorbent, or the space between each adsorbent particle, while the second, multiplied by $1 - \epsilon$, refers to the portion filled by adsorbent, in which adsorption occurs at a quantity q^*.

The smaller this packing factor, the more adsorbent was packed into a container of a given volume, which is attractive and very important in larger-scale projects due to volume and budget restraints. There are, however, theoretical limits depending on the distribution of particle sizes. Packing can be defined based on the number of distinct particle sizes present, from equally sized particles (monomodal), two differing sizes (bimodal), and so on (multimodal). An example of bimodal packing can be seen in figure 4.1.

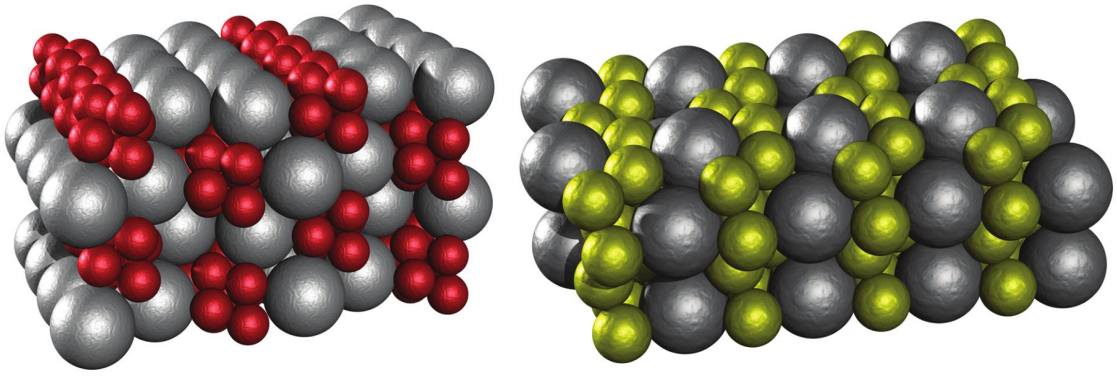

(a) (b)

Figure 4.3: Two illustrative, mathematical examples of a bimodal packing [32] [a].

[a] Reprinted with permission from J. Phys. Chem. C, Vol. 115, nr. 39, pp 19037–19040. Copyright 2011 America Chemical Society.

For monomodal packing, a random packing of spheres uses approximately 64% of space, giving us a packing factor ϵ of 36% [33]. This is the best packing one can expect with a single particle size. For bimodal packing, ϵ goes down to 25%, and it gets lower and lower for an increasing number of particle sizes (multimodal). Bimodal packing is often

the used method due to the fact that the quantity of adsorbent can simply be separated in half – one half is crushed, being then reduced to a much smaller grain, and the other half is unaffected, creating two different particle sizes – and because this simple process increases the packing density by a significant quantity [34].

Rearranging equation 4.2 and using equation 4.1, we can obtain the adsorbed quantity in terms of the system parameters:

$$q^*(P, T_{A/B}) = \frac{\frac{N_{total} - N_{V_2}(P, T_C) - N_{V_1}(P, T_D) - N_{V_0}(P, T_D)}{V_{vessel}} - \epsilon\rho_g(P, T_{A/B})}{(1-\epsilon)\rho_p} \tag{4.5}$$

We have then the defining equation for our system in equation 4.5 and can proceed to the dimensioning, knowing all the involved quantities.

4.2 System dimensioning

Dimensioning of the main components of the system — the adsorption vessel and the calibrated volume — has to take into account the measurement method in use and the extreme conditions when in operation.

The adsorption vessel and the calibrated volume must have dimensions such that the system's pressure variation over the course of a measurement is measurable by the pressure sensors. Essentially, the initial quantity of gas in the calibrated volume has to expand sufficiently into the adsorption vessel so that a significant pressure variation is detected. This creates a compromise: the calibrated volume has to be larger than the adsorption vessel and void volumes, but it cannot be so large that it requires an impracticable quantity of gas for a substantial pressure variation to be read. Using simulated data for neon adsorption on HKUST-1, calculated by J. P. Mota [21], an Excel worksheet was made to gauge this compromise, calculating the pressure difference between two extreme vessel temperatures and system pressures with the results presented in table 4.1.

Table 4.1: Variations of pressure between two extreme vessel temperature and system pressure cases (130 K, 16 bar to 500 K, 100 bar).

V_{vessel}/cm^3	V_{cal}/cm^3	m_{ads}/g	ΔP/bar
7.5	150	4	4.62
7.5	1500	4	0.46

Looking at table 4.1, the values of 7.5 cm^3 and 150 cm^3 were decided on: the pressure variation of approximately 5 bar should be sufficient to carry out the experiment, considering the sensitivity of the pressures sensors used.

4.2.1 Wall thicknesses

The fact that the system will have to hold in pressures up to 100 bar makes it so that some factors that would otherwise be irrelevant become critical — one in particular is the thickness of the walls of the constituents: the adsorption vessel, the involved tubes and the calibrated volume. Failure to accommodate such pressures can result in yield or even fracture of the constituent materials, which could compromise the setup in several ways.

A strength study, implemented in an Excel worksheet, was made on the thickness of walls for cylindrical pressure vessels with hemispherical caps — this shape was chosen due to its structural resilience — applying the thin-wall and thick-wall approaches. The thin-wall approximation assumes that the cylinder walls are infinitely thin in comparison to the diameter, and so it is appliable when the thickness of the wall can be considered sufficiently small in comparison to the diameter. Regardless, we concluded from calculations that it was valid with an error of at most 10% (directly proportional to the maximum allowed pressure) in comparison to the thick-wall assumption, where no

approximations on wall thickness are made. For the thin-wall approximation, the highest stress on a cylinder under internal pressure is the hoop stress, σ_θ, given by [35]:

$$\sigma_\theta = \frac{Pr}{t} \tag{4.6}$$

where P is internal pressure, r the radius of the cylinder, and t the thickness of its walls. This stress is also called circumferential, because it occurs along the circumference of the cylinder's walls.

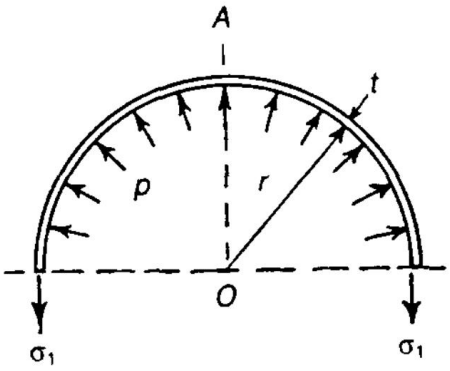

Figure 4.4: Representation of hoop stress, denominated σ_1 [35].

The expression for the thickness is then direct, from equation 4.6:

$$t = \frac{Pr}{\sigma_\theta} \tag{4.7}$$

where, taking into account a limit hoop stress equal to the yield strength of the material in use (as in, the tension required to have the material go into the plastic regime of strain), one can obtain a safe thickness for the cylinder walls of a given material, radius and working pressure. The pressure taken into account was 200 bar, despite the maximum working pressure being 100 bar. This, combined with a security factor of 2 (which gives us a combined safety factor of 4!), is enough to guarantee that the cylinder walls will hold up at the desired working pressures. These calculations were done for every custom part in our setup. For the commercial pieces, such as the tubing and the valves, they were chosen so that their pressure limits largely fulfill our requirements.

When it came to the hemispherical caps, the study was also made. However, the manufacturing of such a shape at the department workshop was considered too complicated in comparison to exaggeratedly thick, flat caps, and so we opted for the latter option. Given the chance, however, these would be structurally sounder and would economize material, which, again, for a larger-scale project would be significant.

4.2.2 Adsorption vessel

The two initial ideas were to either have disposable adsorption vessels or a reusable one with a screw-on cap. The screw would then be tightened and filled with soft solder so as to become leak-tight even at high pressures. The latter idea was opted for, and thus a more detailed strength study was made for the screw in the cap, to determine the thread parameters (figure 4.5) that allowed for large pressures.

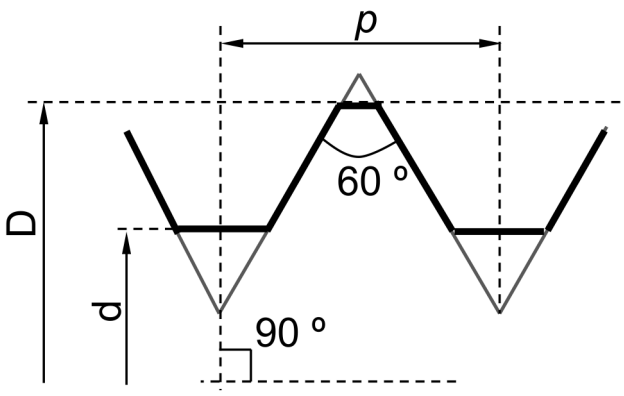

Figure 4.5: Representation of thread parameters: p the pitch, D the major diameter and d the minor diameter [36].

The stress on one given screw can be calculated as (F is the force, S the surface):

$$\sigma_{screw_1} = \frac{F}{S} = \frac{4F}{\pi(D^2 - d^2)} \tag{4.8}$$

With the stress distributed over a given number N of screws being:

$$\sigma_{screws} = \frac{\sigma_{screw_1}}{N} = \frac{p}{H}\frac{4F}{\pi(D^2 - d^2)} \tag{4.9}$$

A regular thread of 1 mm pitch p over 10 mm length H proved no issue, with a stress of 6.8 MPa in comparison to the usual approximate yield strength of copper, 70 MPa.

To validate this design, a dummy vessel (slightly shorter than the final version) was built to perform a burst pressure test with water, using a high pressure generator and a pressure sensor (up to 300 bar). Let us note that this test was done with water for safety reasons: a gas burst is much more destructive than a water burst, due to the higher compressibility of gases.

The copper dummy vessel had a radius of 9 mm, and consequently, according to equation 4.7, a wall thickness of around 5 mm. The test also had the intent to test out the hypothesis that the vessel should hold under pressures of 200 bar, for which it was dimensioned.

Internal pressures of up to 280 bar were applied, with no visible yield, fracture, or leakage of the vessel. As the available pressure sensor was limited to 300 bar, the test was

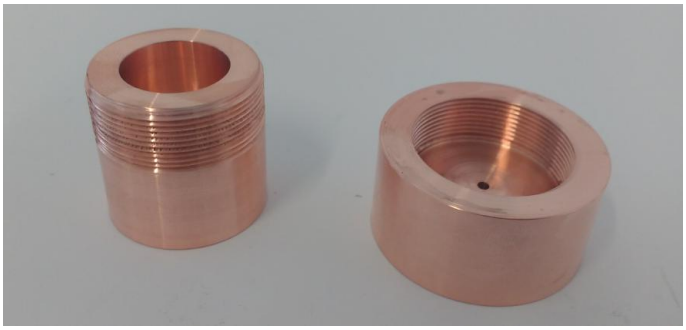

Figure 4.6: The dummy vessel built for pressure testing.

considered finished, with positive results: the vessel holds up in pressures at least almost three times as high as the maximum working pressure of around 100 bar!

After this design was considered validated in terms of pressure, the drawing of the final version was possible. There were a few changes compared to the dummy vessel: the vessel was made longer to increase its volume to the projected 7.5 cm^3 from table 4.1, holes were made to tightly accommodate both the 50 W heating resistor and the two Pt100 thermometers, and a support system was designed to hold the vessel to the gas manifold, protect the thin capillary that connected the two, and allow the wiring of the vessel resistors to the room-temperature adapter. The final version can be seen in figures 4.7 (which will be described below) and 4.8 (b).

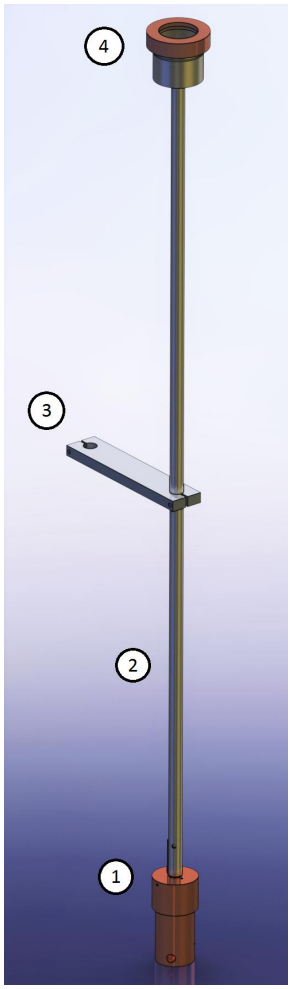

Figure 4.7: A 3D view of the support system.

A stainless steel tube (2) was brazed on one extremity to the brass piece that's screwed on top of the vessel (1), and on the other to a 12-pin connector adapter (4) for the temperature controller. This allowed us to wire the thermometers and heater mostly through this tube, greatly protecting the wiring.

To add on to this, an aluminum piece (3) was manufactured to hold the capillary's manifold connection to the stainless steel tube, as well as fix the whole support system to the manifold (see figure 4.8 (b)).

Why a very thin capillary? Since the vessel temperature is going to vary between 77 K and 500 K and the manifold will be always at room temperature, there will often be a very large temperature gradient in the capillary connecting the vessel to the manifold: a minimization of this volume to the point that it is almost negligible will reduce possible errors in the calculation of its gas quantity. The capillary that was mounted in the system had an inner diameter of 0.8 mm and a length of 400 mm: it had an approximate volume of 0.2 cm^3, vastly inferior to any other volume in the system. The fact that it is negligible

doesn't necessarily mean that it doesn't factor into calculations – an average temperature between the vessel and the manifold was taken for this volume and considered in the final calculations, despite having little effect in the results.

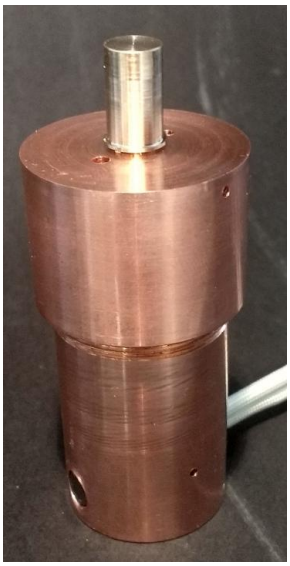

(a)

(b)

Figure 4.8: In (a), the final version of the vessel. Note the smaller holes for Pt100 thermometers. In (b), the support system mounted on the manifold, to be compared to figure 4.7.

The volume of this final vessel (figure 4.8, (a)) was then measured to confirm our initial projection. The measurements were done by weighing the vessel, both completely empty and completely filled with distilled water, and taking the difference as the mass of water inside. This can then directly be converted to the volume of water inside. The drawing had a volume of 7.634 cm^3, while the measurement yielded 7.63 cm^3, leading us then to conclude that we could use this value as a constant for the rest of the work to be carried out and that we had been able to determine a very important volume for the proper functioning of our method.

4.2.3 Calibrated volume

One solution initially thought out for the calibrated volume was the acquisition of a diving cylinder. These diving cylinders withstand up to 300 bar and typically have an internal volume of 3 to 18 L. However, no compatible sizes were commercially available considering the projected dimensions in table 4.1.

Figure 4.9: The calibrated volume, with the mounted thermometer C.

The calibrated volume was able to be manufactured in our workshop, from a 316 stainless steel rod, which saved us time and resources. The drawing was done to obtain a piece that would hold, as per table 4.1, around 150 cm^3. Considering the usable length of material we had, the determined inner radius for the volume was 21 mm, which brought the thickness to (again, as per equation 4.7) around 4 mm. The length was calculated to be 108.3 mm. It's interesting to notice how much stronger stainless steel is than copper: a vessel with more than double the radius has 20% less thickness for the same pressure requirements due to the relatively higher yield strength. The piece was made in three separate parts: the body, and two caps to be brazed on each side, so as to close the hollow cylinder. A 1/4 inch tube with a standard connector was then brazed to the holed cap so that the calibrated volume could be connected to the gas manifold. An attempt at measuring the volume through water weight was made after all pieces of the calibrated volume were welded. Unfortunately, the complete filling of the volume with water through the small tube proved more complicated than initially predicted, as air bubbles could be heard as it was shaken and the volume results were highly variant and lower than initially predicted. In hindsight, a suitable solution would be to have done this prior to the brazing of the top cap, which would simplify the filling. The final capacity measurement had to then be performed through gas expansion, section 4.7.

A Pt100 thermometer was then installed and thermally coupled to the calibrated volume, and this volume was thermally insulated (from outer influences such as air currents, or even liquid nitrogen vapor from the cold reservoir), so as to have an accurate, fluctuation-free temperature measurement, allowing an accurate determination of the gas quantity.

4.3 Vessel filling and preparation

For the adsorption vessel to be ready for the introduction of the sample, mounting of the resistors and soldering of the cap (a process which was repeated several times over the course of this work), it must be thoroughly clean. This was done initially by hand to remove any obvious moisture and finalized with an ultrasonic bath, set to 10 minutes using acetone. This cleaning procedure is important for the inner part of the vessel, which will be in contact with the sample, but also for the outer threaded part, in order to allow a good wetting of the screw to be soldered.

Filling the vessel with HKUST-1 has to be a careful process, as the material is toxic and ours had a very small grain size of 16 µm (see table 2.1), meaning it behaved almost like very light dust. Thus, protective equipment such as glasses, gloves and a dust mask are advised, as well as careful handling. The material doesn't seem to adhere at all to paper, which makes it a suitable base to carry out the filling. The greatest possible amount of adsorbent has to be put into the vessel, which requires mechanical vibrations by hand on the vessel as the filling is done, to force the sample to fully settle (as best as possible) in the free space beneath it. Further compression was made with a metal piece to attempt a greater degree of packing. The vessel was weighed before and after this process to determine the mass of sample that had been packed into it.

Figure 4.10: The vessel, post-filling.

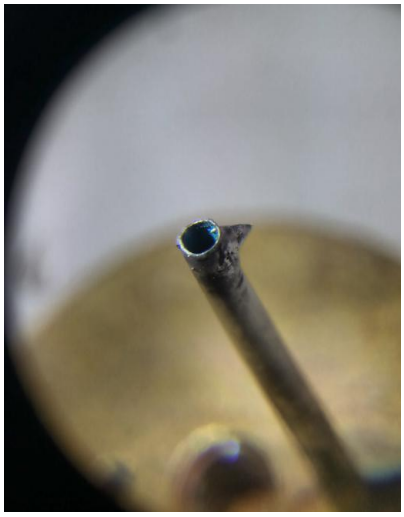

Figure 4.11: Vestigial amounts of HKUST-1 outside the vessel.

To prevent the sample from leaving the vessel as pumping or fast gas discharges occur, some type of filter had to be applied. The choice fell on a stainless steel grid with 25 µm holes as well as a small quantity of glass wool in the tube exiting the vessel's cap. This quantity of glass wool is crucial, as an initial experiment with only the aluminum grid had us discover that the sample left the vessel quite easily (figure 4.11, in light blue). This forced us to clean out the system, as we had pumped a small quantity of sample.

The cap is then tightly screwed on and the complete vessel exposed to a pre-activation period in order to remove unwanted moisture from the sample. After staying overnight at 80 ºC in a low vacuum, the muffle oven is filled with nitrogen to prevent adsorptions of other species present in air. After this process, the vessel is weighed to confirm the quantity inside (small variations of mass might occur in activation, figure 3.2). The vessel's screw is then ready to be filled with solder.

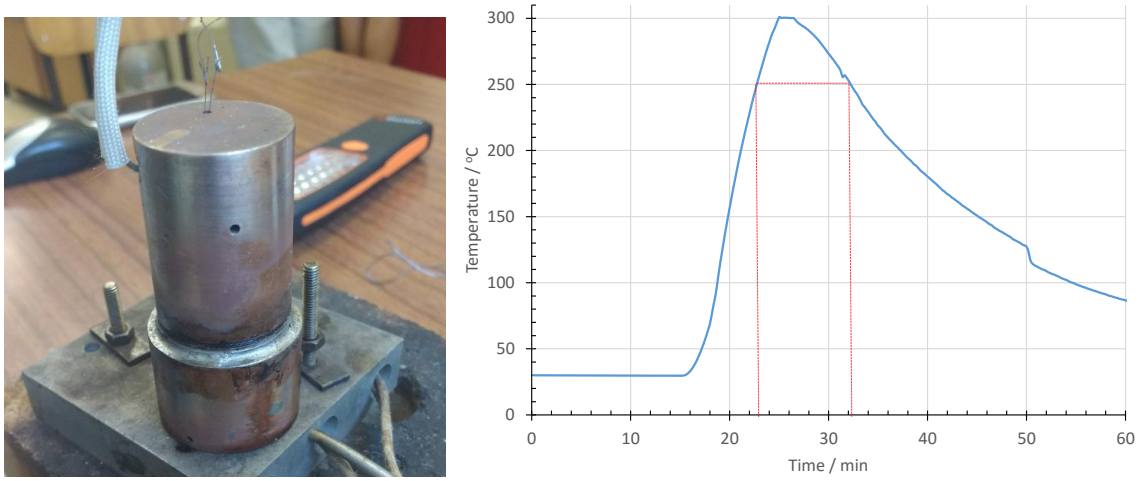

(a) (b)

Figure 4.12: In (a), the system for controlled soldering. Not shown is a glass wool cap on the top of the vessel to lower cooling by convection. Note the (good) final aspect of the solder bead. In (b), temperature vs. time for the process.

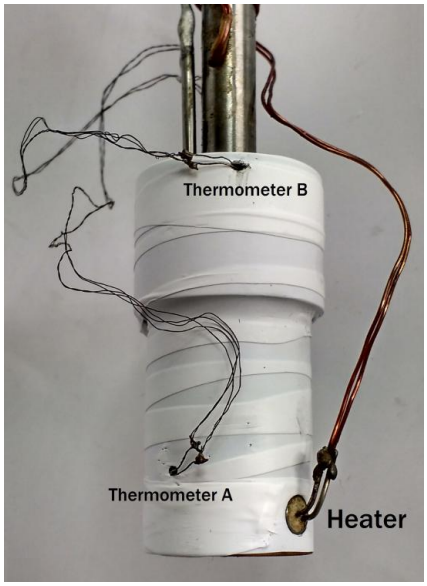

Figure 4.13: The vessel with its thermometers and heating resistor. A second layer of teflon was applied before the insulation to fix and protect the wiring.

This soldering process, in the case of high-temperature solders (above 250 ºC), has to be controlled due to the sensibility of HKUST-1 to temperatures above 300 ºC (see figure 3.2). With this in mind, a small set-up for a well-controlled and uniform soldering process was made (figure 4.12), which allowed for a high degree of control and for the process to be done in less than 10 minutes, which is positive because the sample was only at high temperatures for a relatively short time.

After this, the thermometers and heating resistor can be mounted in the vessel and isolated electrically with teflon tape (melting point: 600 K) (figure 4.13). The designations for the thermometers in the figure are identical to the ones in figure 4.1.

The vessel is then mounted in the manifold and activated at 150 ºC (423 K, see table 2.1) in a low vacuum (less than 1 mbar). This proved to have some disadvantages, as will be discussed in subsection 5.3.1.

For the total results presented in section 5.1, the screw soldering process was not the one described here for high temperature solders, because the thread was filled with regular 180 ºC (453 K) Sn electronics solder at an initial stage, to avoid damaging the sample at higher temperatures (figure 3.2). A later attempt with 296 ºC (569 K) Pb solder was made (figure 4.12 (a)) to try to reach 500 K measurements.

4.4 LabVIEW^{TM} interface

The system's interface was developed in LabVIEW^{TM}, adapted from a previous interface already implemented by Gonçalo Tomás for thermal conductivity measurements of porous copper [37].

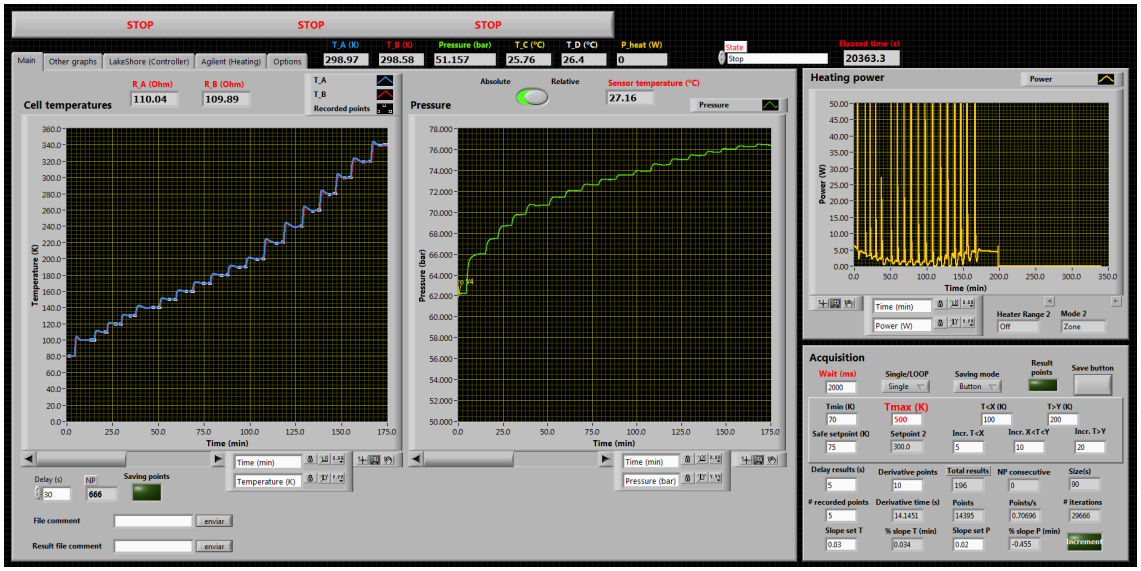

Figure 4.14: The LabVIEW^{TM} interface's main tab.

Its function is to provide a visualization of the important parameters such as pressure, heating power and all the mounted thermometers' readings, as well as some other features: automatic acquisition, temperature control, result and log file output and pressure vs. temperature graphs for real-time analysis, allowing early detection of possible system anomalies.

The aspect that is less trivial and more interesting to note is the equilibrium detection algorithm: it calculates the slope of a given number of acquired points and constantly compares it to a stabilization criterion set by the user. In our case, it does this for both temperature and pressure, the parameters that should be constant at an equilibrium, acquiring a given number of points that satisfy these criteria in a row. Then, when the designated number of stable points is uninterruptedly obtained, they're registered in a file and an increment to the controller's temperature setpoint occurs, leading the interface to then repeat the process at another temperature point.

The result of the application of this algorithm can be seen in figure 4.14, where automatic stabilizations were achieved with a slope criterion of 0.03% for temperature and 0.02% for pressure, as well as in any other measurement cycles shown in the document. Further results will be seen in figure 4.17 and all over chapter 5, with mostly the same criteria, which were found to work seamlessly.

4.5 Cooling and heating system

As already mentioned in subsection 4.2.2, two Pt100 thermometers and a 50 W heating resistor make up the sensing and heating part of the developed cooling and heating system, respectively. The used temperature controller was a LakeShore 336 model, interfaced with the LabVIEW^{TM} program introduced in the previous section.

Simply cooling is a relatively simple task, as surrounding the vessel with liquid nitrogen will very quickly thermalize it to around 77 K. Accurately controlling the temperature through heating against a liquid nitrogen reservoir from 77 K to 500 K is, however, a completely different challenge. The vessel has to be insulated from the cold source to the point where its temperature can be raised, but not too insulated so that it allows enough cooling power for temperature control to be possible.

Several experiments were made to adjust this thermal insulation before we arrived at a functioning system. The first idea was to use spray polyurethane foam, often used in houses for wall insulation, as a means to thermally insulate the vessel: covering it with aluminum foil, applying the foam and waiting for it to polymerize. This did not exactly function well, as heating was very inefficient and wasted large quantities of liquid nitrogen: stabilizing at 300 K required over 40 W of heating power, which in principle made it quite complicated to reach 500 K. This was probably due to the abundance of large channels in the polymerized foam, in which liquid could penetrate (figure 4.15, leftmost).

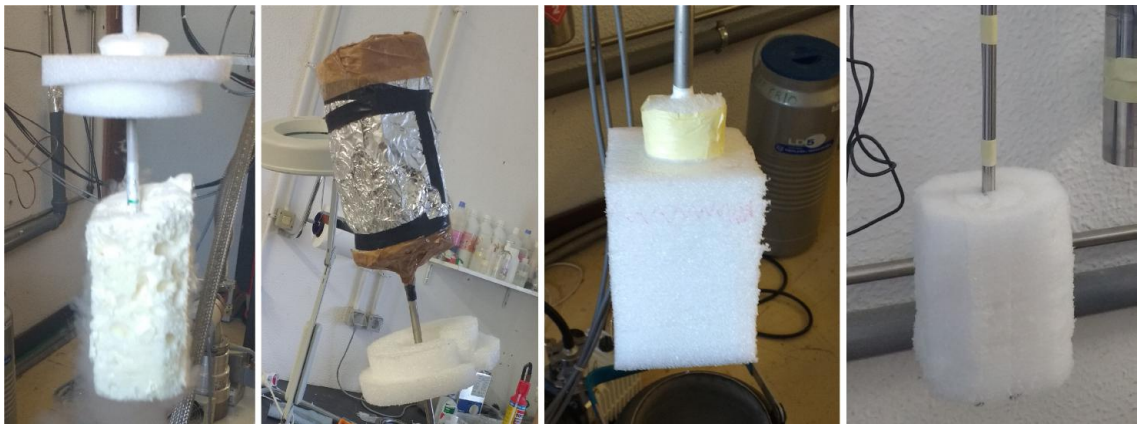

Figure 4.15: From left to right, the first to final iterations of the vessel's thermal insulation.

The second and third iterations tried to solve this by wrapping the expanding foam casing in aluminum foil, which proved fragile: the foil became especially brittle at lower temperatures (figure 4.15, second picture).

Finally, we decided to give up on the expanding foam and use plastic packing foam instead, which proved to be significantly better in terms of thermal insulation. However, the addition that made this new plastic foam casing viable was the wrapping of the vessel in glass wool: the plastic foam started decomposing if in direct contact with the vessel,

when high temperatures were applied. Glass wool is an insulating material made from fibres of glass and has a texture similar to wool, which makes it highly malleable and adaptable to different shapes. This was enough to properly insulate the vessel but still allow it to cool down to our reservoir's 77 K. A custom vessel-sized casing was then carved, with some help from the workshop, to house the glass wool-wrapped vessel for heating and cooling tests (figure 4.15, rightmost). A diagram can be seen in figure 4.16:

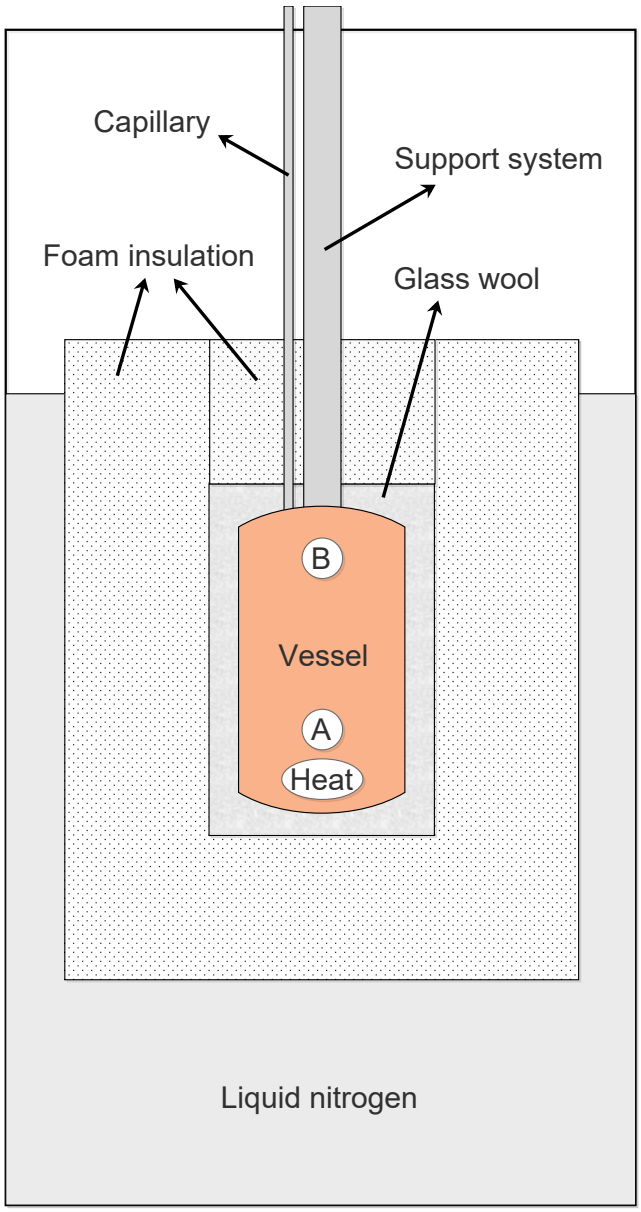

Figure 4.16: A diagram of the final version of the heating and cooling system, as seen inside the dewar. The vessel is protected by the glass wool and foam insulation from the liquid nitrogen, and held in place by the support system detailed in subsection 4.2.2. Not shown but implicit is the teflon protection from figure 4.13. The thermometers (A and B) and the heating cartridge (Heat) positions are represented.

These tests consisted of programming the temperature controller's PID (proportional-integral-differential) parameters. These parameters are coefficients in the PID mechanism, which consists of the calculation of the difference between a desired setpoint and a measured process variable (in our case, the temperature), denominated error value. It then attempts to minimize this difference by adjusting a control variable (in our case, the heating power). The name of this mechanism comes from the expression that rules over it:

$$u(t) = Pe(t) + I\int_0^t e(\tau)d\tau + D\frac{de(t)}{dt} \tag{4.10}$$

where $u(t)$ is the control variable value, e the error value, P the proportional coefficient, I the integral coefficient, and D the differential coefficient. These three coefficients were determined by trial-and-error, so that the stabilization occurred within a reasonable time-frame. Over such a large temperature range (77 K to 500 K), it's often not enough to define a single group of these three values due to the large variation of thermal properties in this temperature range: in our case, 3 different regions had to be defined and so a total of 9 coefficients had to be determined in a trial-and-error process. More practical results can be observed in the next page, figure 4.17. Stabilization in temperature was able to be done to the third decimal place given enough time!

Considering the temperature target (500 K or 223 ºC), the solder used in the sensors and heater could not be a typical Sn solder (180 ºC fusion point). Therefore, these components were welded with a Pb solder (93%), containing also small amounts of Sn (5%) and Ag (2%), with a fusion point of 296 ºC, which is widely above our temperature limit and so it doesn't risk any desoldering.

Cooling down the vessel usually took around 20 minutes, whereas fulfilling a full heating cycle from 77 K to 500 K took the system as long as 4 hours, depending on the amount of setpoints used. This is appreciable, since, concerning the volumetric method, a handful of cycles at different pressures are enough to trace out isotherms over a relatively wide range, which was the final goal of this work.

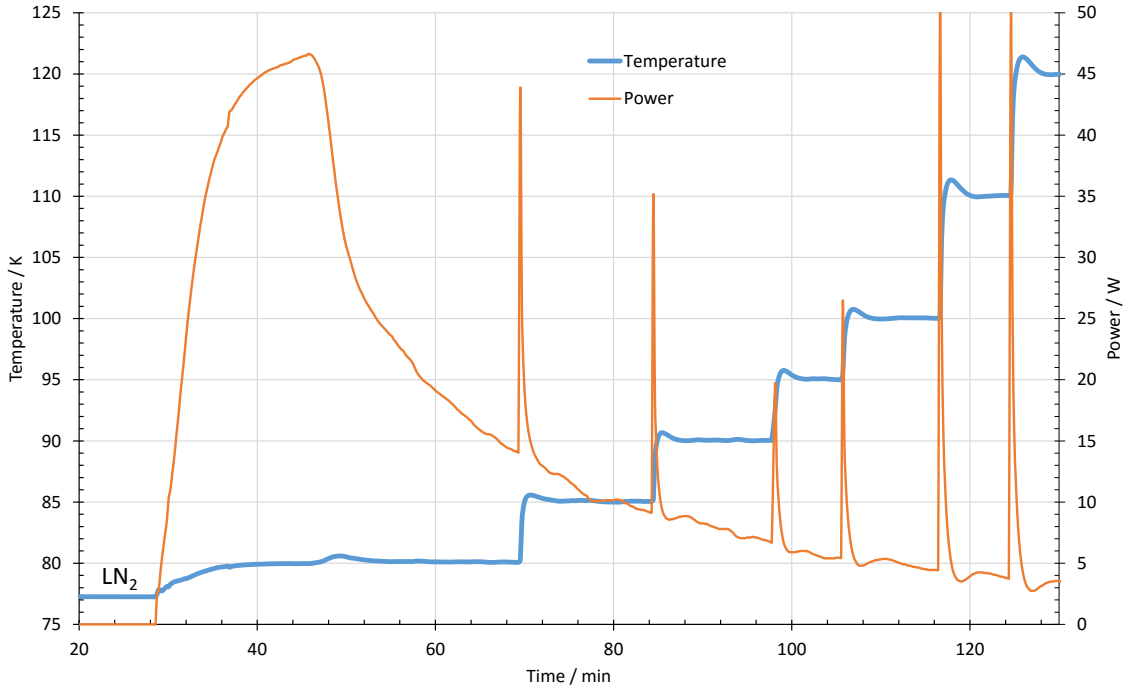

(a)

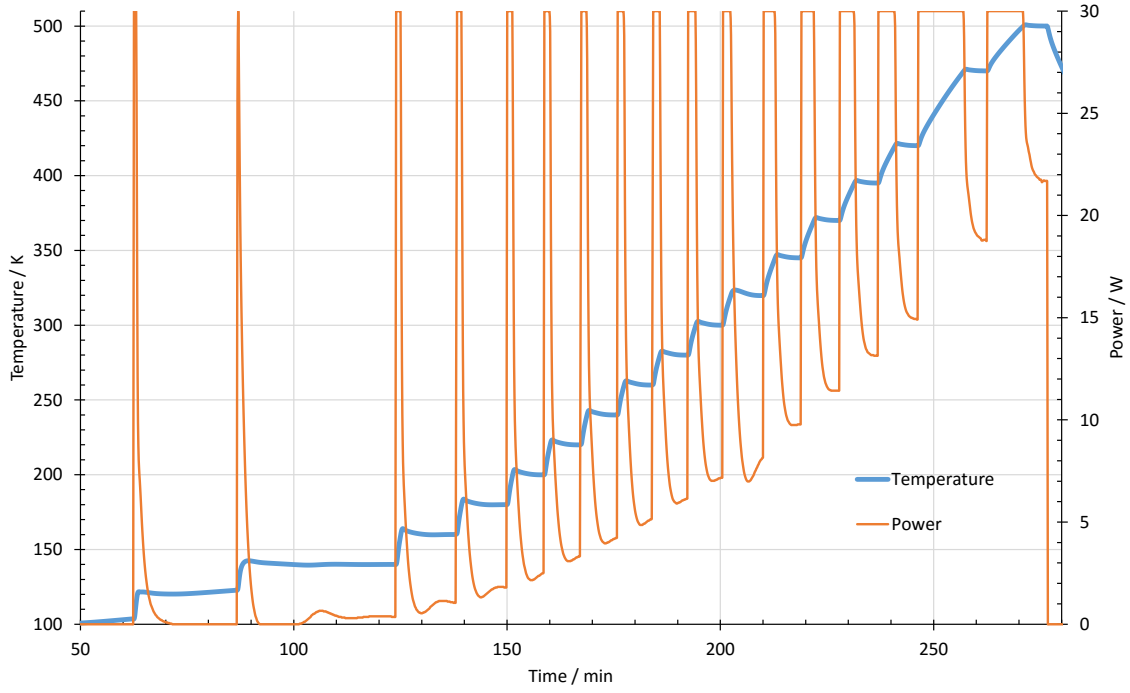

(b)

Figure 4.17: An example of temperature stabilizations in the whole temperature range, lower in (a) and higher in (b), with a temperature slope criterion of 0.03%. Notice the heating peaks and following stabilization in temperature. The vessel was empty for these tests.

4.6 Experimental procedure

Two specific variations of the volumetric method were initially discussed to perform the experiments, and they will be illustrated in the pages that follow.

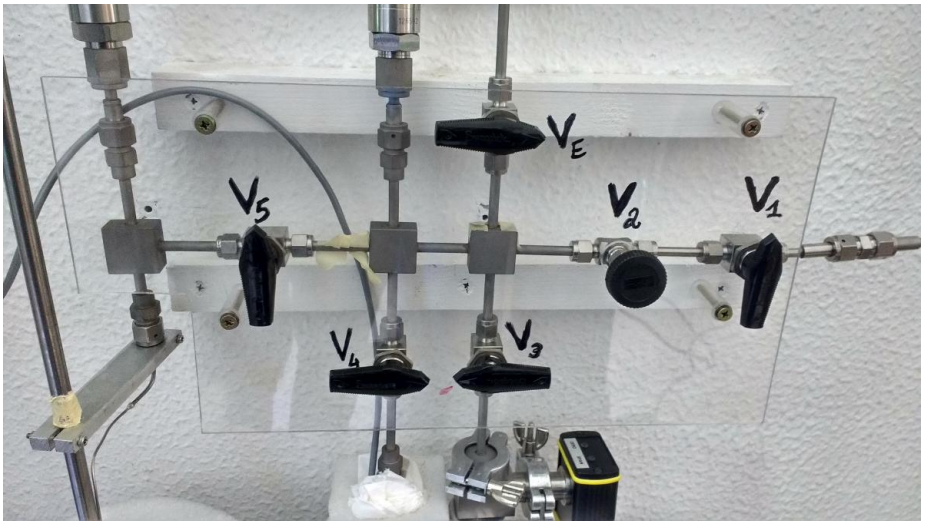

Figure 4.18: The manifold, fully wall mounted. Compare to figure 4.1 and note the support system described in subsection 4.2.2, figure 4.7, on the left after valve 5, as well as the insulation for the calibrated volume described in 4.2.3, after valve 4 in the bottom.

The first discussed procedure, A, is the most similar to the volumetric method described in the state of the art. A measurement should be made through these steps:

1. Cleaning phase: with the gas supply closed (valves 1 and 2) and the rest completely open, the system is pumped to a low vacuum (less than 1 mbar).
2. Filling of the calibrated volume: closing valves 3 and 5 and opening valve 1, open valve 2 to a given initial pressure P_i. Measuring the pressure and temperature of the calibrated volume, the total amount of gas in the calibrated volume at that time, and in total for the whole system after step 3, can be determined. Close valve 4 and pump the system, except the calibrated volume.
3. Expansion to vessel and measurement: expansion by opening valves 4 and 5. The vessel can then be set to a temperature and the pressure read over a given period of time, giving us access to the adsorbed quantity of gas dependent on pressure for a given vessel temperature.
4. Stabilized heating cycle: to obtain a set of various q^* points, sweep vessel temperature setpoints from 77 K to 500 K (see, for instance, figure 4.17). This gives access to adsorption curves, quantity versus temperature and pressure.

A variation of this first procedure, B, arose for the emulation of an actual adsorption compressor, capable of very large pressure differences. The calibrated volume is removed

(i.e., valve 4 permanently closed), making V_0 and V_1 the actual "calibrated volume". This setup is the most possibly similar to the first phase (pre-heating) of an adsorption compressor's functioning cycle.

The procedure is essentially identical in terms of setup, excluding valve 4 and the calibrated volume from procedure A. Instead of carrying out an expansion, the gas resides in only V_0, V_1 and the adsorption vessel. We will later be able to observe that, since the room temperature volume is much smaller, adsorption and desorption will lead to considerably larger pressure variations.

Procedure A was the most used one: the big disadvantage in procedure B is caused by the absence of the calibrated volume as a buffer. The capillary's volume becomes much more significant in comparison to the total system volume, which means an error in its temperature (which is inevitable, due to a very large gradient along it) becomes an actual issue. Through the same rationale, an error in the determination of V_1 is now also much more significant in a relative way, which also induces greater, unpredictable errors in the results. A comparison of results obtained with both these procedures will be made in chapter 5 and the conclusions will be similar.

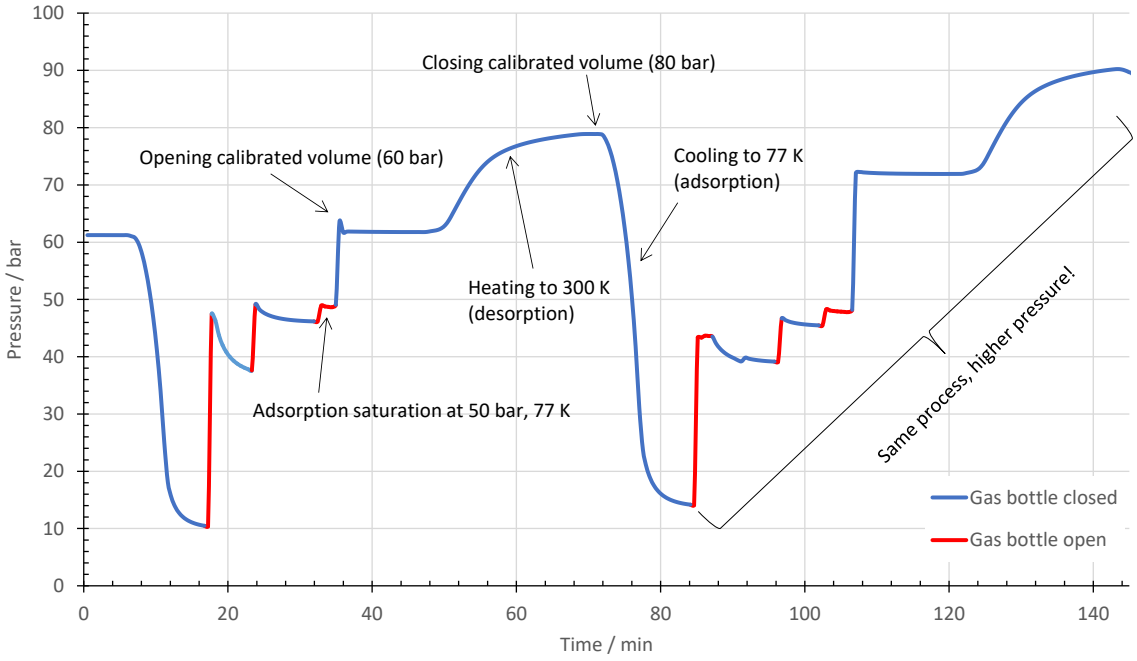

Figure 4.19: The method to go beyond the bottle's pressure.

A procedure for filling the calibrated volume arose because the pressure in the neon bottle was about 60 bar, and its pressure reducer was limited to 70 bar. To circumvent these limitations, the vessel filled with HKUST-1 was used as a thermal compressor, through heating cycles between 77 K and 300 K, in order to fill the calibrated volume with a desired pressure above our bottle and reducer limits. In short, a cycle of adsorbent saturation (through cooling) and neon desorption (through heating) raises the pressure in the calibrated volume. The different steps are detailed in figure 4.19.

4.7 Determination of system volumes

The determination of the main volumes in the system was, as already detailed in section 4.1, the most critical part to properly interpreting the obtained data.

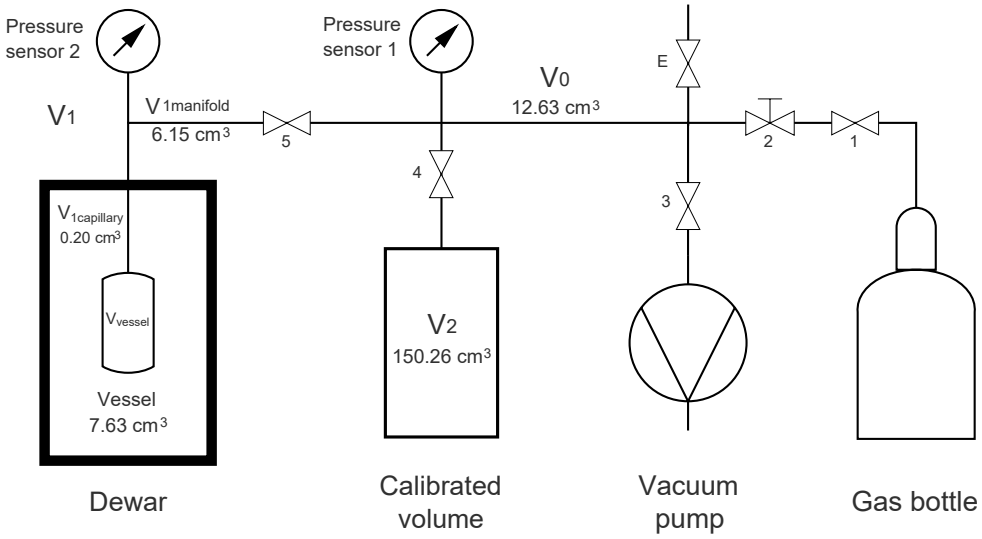

Figure 4.20: The volume designations in the system and their capacity, determined as explained in the text below.

There are several ways to achieve an accurate determination of the volume capacity. Perhaps the most simple is a gas expansion from a calibrated volume to the volume we wish to determine. Through two pressure measurements, one can accurately and quickly determine the total volume and thus the variation in volume, correspondent to the value we want to find out. Assuming a closed system and constant temperature:

$$N_i = N_f \rightarrow P_i V_c = P_f (V_c + V_?) \rightarrow V_? = \left(\frac{P_i}{P_f} - 1 \right) V_c \tag{4.11}$$

where V_c is a calibrated volume, $V_?$ the volume we wish to determine, and P_i and P_f the pressures values before and after the expansion, respectively.

However, when one does not have a well-calibrated volume available to do this simple process, another possibility is to use a known volume variation to obtain a well-calibrated volume in a system. To this effect, an adjustable calibrated volume was borrowed from the METROVAC laboratory at FCT-UNL. From its measurements (3.1 cm diameter, 0.175 cm screw pitch), we could calculate the volume variation per turn of the adjustable wheel. In this case, the calibrated variable is not the volume, but the variation in volume when the adjustable wheel is turned:

$$V_{turn} = \pi \left(\frac{3.1}{2} \right)^2 0.175 = 1.245\,\mathrm{cm}^3 \tag{4.12}$$

The volume most easily determined through this method, due to accessibility, was V_0, the central volume in the manifold. It's then simple to apply equation 4.11 but for a variation in volume ΔV, with V_c the calibrated volume's initial capacity, which is also unknown:

$$P_i(V_c + V_0) = P_f(V_c + V_0 + \Delta V) \rightarrow V_c + V_0 = \left(\frac{P_f}{P_i - P_f}\right)\Delta V \quad (4.13)$$

This leaves us with knowledge of the volume we want to know, V_0, added to the initial calibrated volume that we in principle do not know, V_c. We can, however, with current knowledge of the pressure, close the calibrated volume's valve and pump V_0, do yet another expansion, now from the calibrated volume to the volume to be determined. V_c is then given by:

$$P_i(V_c+\Delta V) = P_f(V_c+V_0+\Delta V) \rightarrow V_c = \frac{P_f}{P_i}(V_c+V_0+\Delta V)-\Delta V \quad (4.14)$$

Having determined the initial calibrated volume V_c, from equation 4.14 and having knowledge of the total initial volume $V_c + V_0$ from equation 4.13, we can subtract one from the other and obtain V_0. This was done through both compression and expansion of the calibrated volume over 20 times to accumulate statistics, giving us a very well-defined volume.

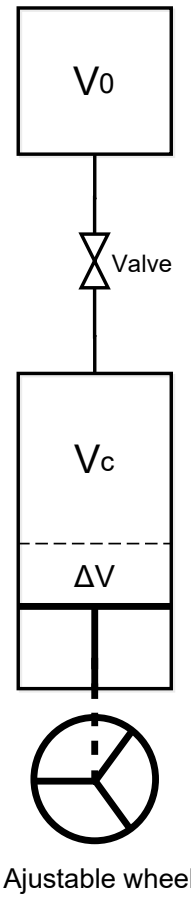

Figure 4.21: A diagram of the method for V_0.

From here, V_0 could be used as the calibrated volume for expansions carried out into the other volumes to be determined, by equation 4.11: V_1 and V_2 were both determined through this method. The obtained values after this volume determination are indicated in figure 4.20. These values were considered constant for the rest of the work done, as there was a great deal of confidence in V_0: the volumes determined from expansions starting in it should then be correct. This is due to the great amount of measurements done with the adjustable calibrated volume and to the relative precision of a standard gas expansion: the process is instant and the only significant error to be taken into account is of a pressure reading. The resolution of the pressure sensor (0.002% of the 10 bar absolute full scale, which is 0.2 mbar), which had been zeroed in a vacuum, was quite good, which leaves us confident in the pressure (and consequently volume) measurements carried out.

It's also worth mentioning that extensive leak testing was performed in this initial phase, so as to minimize any possible losses of gas, which would greatly affect both the method and our initial calculation of V_0, as these are relatively lengthy processes. This length could have been significantly reduced if a careful measurement of the calibrated volume's capacity had been done before the caps were welded.

4.8 Empty-vessel tests

With the intention to confirm the volumes determined in the previous section, some tests with helium as a working gas were made, with no sample inside the vessel.

The idea was to use the mass balance equation 4.1 to, after knowing the total quantity of helium in the system, calculate the portion in the adsorption vessel. Comparing it with the real quantity present at the measured temperature and pressure through NIST's REFPROP [38], we can then deduce the error that is being made through this mass balance calculation. Moreover, these tests were used to test silicone paste as a leak-tight screw seal for high pressures and low temperatures, instead of soft solder.

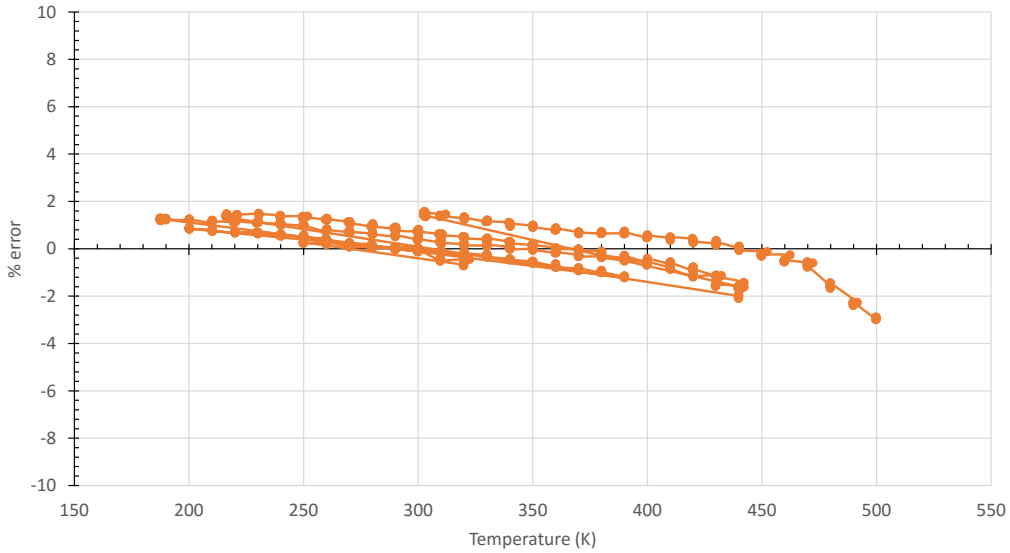

(a)

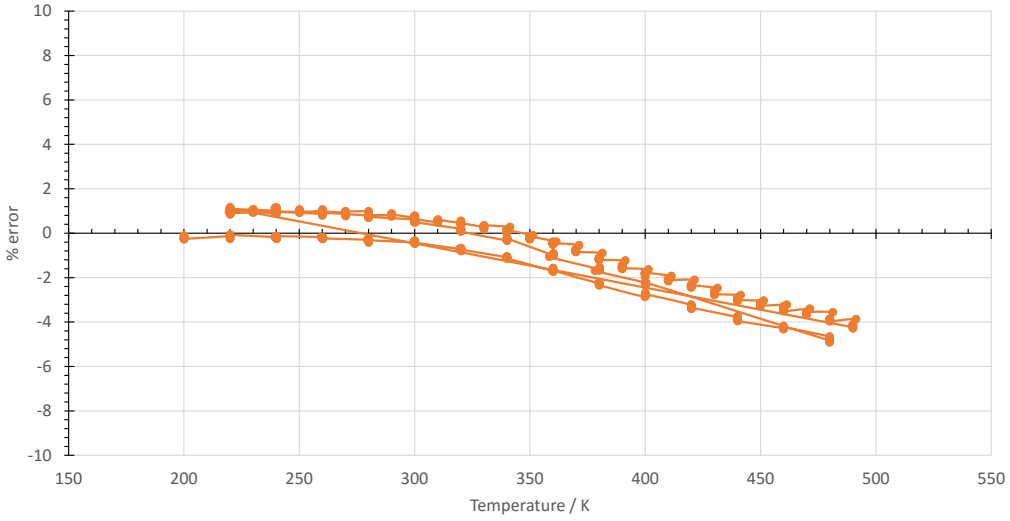

(b)

Figure 4.22: The relative error of ideal vs. real (REFPROP) gas quantity in the vessel for several heating cycles done at circa 2 bar for the first, (a), and second, (b), silicon tries.

In essence, the relative error represented in figure 4.22 is:

$$\rho_{vessel} = \frac{N_{vessel}}{V_{vessel}} = \frac{N_{total} - N_{V_0} - N_{V_1} - N_{V_2}}{V_{vessel}} \tag{4.15}$$

As we can observe in figure 4.22, the best results were all mostly in range of 2% error for the first try and 4% error for the second, which is a decent mark for volumetric measurements. Some other results were taken, including at higher pressures, but the ones presented above exhibited the best reproducibility. Other results went up to 5% error only in the higher temperature range (400 K to 500 K), which proved difficult to understand and solve.

This motivated us to not to take many conclusions from these tests due to not understanding these variations.

Figure 4.23: The silicone excess in the second round.

For these tests, some experiments on sealing the screw with high temperature resistant silicone were made. Two tries were made: for the second try, some irregular results (not presented here) led us to conclude that we had exaggerated in the used quantity and thus reduced the vessel volume through an excess of silicone on the inside, which proved true as we opened it up (figure 4.23). This might explain the bigger maximum error in the second try. We found that the silicone repeatedly leaked above 5 bar internal pressure, which restrained our empty-vessel studies to low pressures. This motivated us to move on to testing on a sample and discard the possibility of silicone for the thread filling. Regarding the minimum tested temperature of 200 K: we weren't sure that the silicone would behave properly at 77 K and therefore, since we instantly stopped after realizing it wasn't suited for high pressures, we did not perform measurements below 200 K.

As such, we considered that the system was ready to obtain adsorption results on HKUST-1. In the next chapter we will look back in a critical way, exposing, analyzing and discussing these results and what possible factors from our dimensioning and preparation detailed in this chapter 4 could impact them positively or negatively.

Chapter 5

Results and analysis

5.1 Neon on HKUST-1 adsorption isotherms

The results were treated using an Excel worksheet programmed for automatic result analysis and tracing of isotherms, using equation 4.5. For any and all result treatment done in this chapter, the real (as opposed to ideal) gas quantities at given temperatures and pressures were given by NIST's REFPROP [38], to avoid unnecessary errors, even if minimal in certain ranges. Initially, the treatment had been done with the ideal gas equation but at higher temperatures and pressures the compressibility factor Z of neon differs by up to 4%, which is enough to induce significant errors in adsorption quantity. An example will be given in subsection 5.3.2.

Another source of errors, since we're working in a quite large temperature and pressure range, is the expansion and contraction of the vessel due to temperature and/or pressure. The variation of the vessel's volume due to variation in its temperature was then accounted for, using copper dilation data from NIST [39]. Between 77 K and 500 K the vessel volume varies by around 0.15 cm^3, which can induce an error of up to 2% in the adsorption quantity. Calculations on the volume variation due to pressure were made, but the contribution was insignificant. A table summarizing the percentual influence of errors in volume determination, mass determination, the real gas correction, and the thermal expansion correction, will be presented in subsection 5.3.1.

An aspect worth revisiting is the packing factor ϵ (section 4.1), and how much adsorbent we were able to pack into our adsorption vessel, for the reasons already explained. Keeping in mind that the distribution of our commercial HKUST-1 was monomodal (16 µm particle size, table 2.1), the best ϵ we could realistically achieve was 36%, which means 64% of the vessel is filled by HKUST-1. As such, we made several packing attempts in which we attempted to pack the most possible HKUST-1 into our

vessel, as per the procedure in section 4.3. For the total results presented in this section, ϵ was 45%, corresponding to an adsorbent mass of 3.955 g. Our best result, however, was a packing factor ϵ of 42%, for the last, short experiment presented in the next section, which corresponded to an adsorbent mass of 4.165 g.

For a single measurement session, following procedure A outlined in 4.6, the temperature was varied from 77 K to 400 K, obtaining the results in figure 5.1 (b).

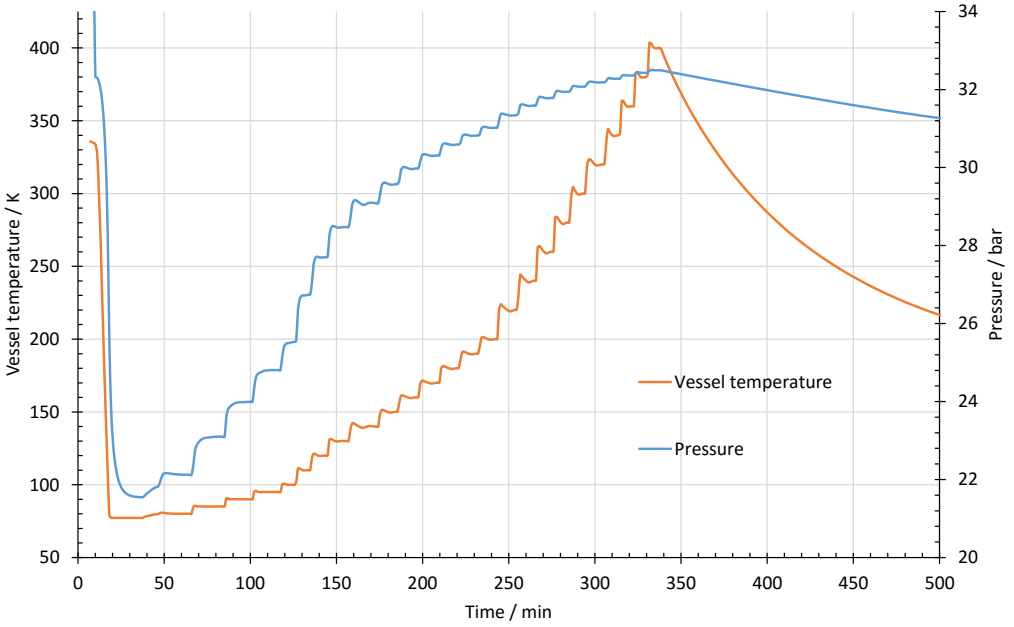

(a)

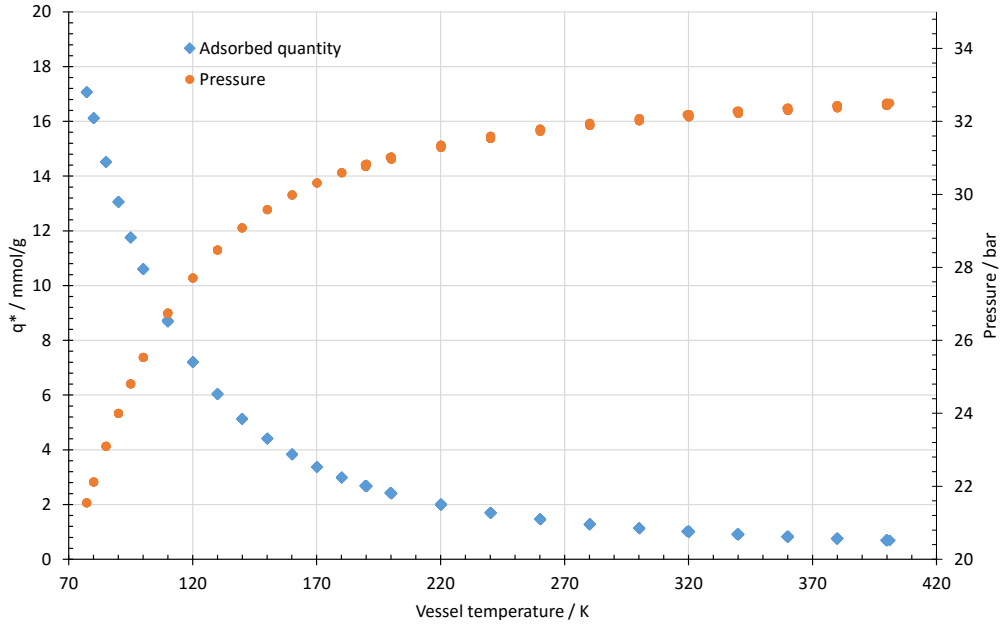

(b)

Figure 5.1: System parameters and results for a session. In (a), variations of pressure and vessel temperature. In (b), adsorbed quantity and pressure vs. vessel temperature.

In this figure, for an initial calibrated volume filling pressure of around 38 bar, it's interesting to notice how the system pressure follows the vessel temperature very strongly due to adsorption. We can further observe the effect in the pressure: from 77 K to 300 K and for a total system volume of around 175 cm^3, there's a compression of 12 bar, from 20 bar to 32 bar.

Seven other sessions, similar to the one presented above but at different initial calibrated volume filling pressures (from 5 bar up to 76 bar), were performed to cover a wide pressure range.

To trace out an isothermic curve (i. e. the quantity of adsorbed gas vs. pressure at a fixed temperature), we must always use the same temperature setpoints for the automatic control (see sections 4.4 and 4.5) in different measurement sessions, which will then be the temperatures corresponding to our different isotherms. The intervals decided on were, in short: after the initial setpoint of 77 K (thermalized with liquid nitrogen), from 80 K to 100 K in 5 K intervals, from 100 K to 200 K in 10 K intervals, and from 200 K on in 20 K intervals.

With this in consideration, the total results taken are presented in the next two pages, in the form of isotherms (figures 5.2 and 5.3).

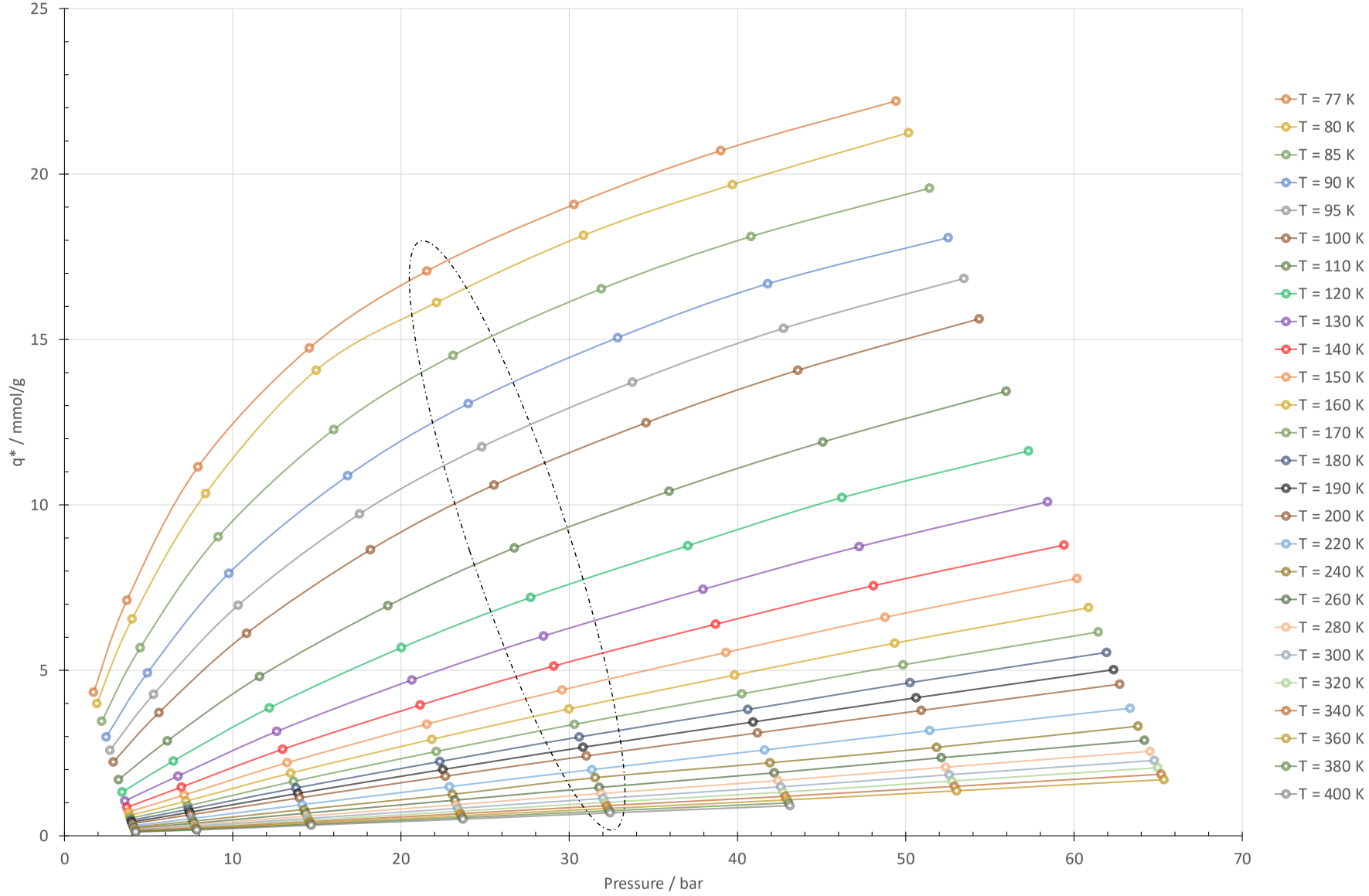

Figure 5.2: The total adsorption isotherms up to 400 K. Outlined is the set of results from figure 5.1 (b).

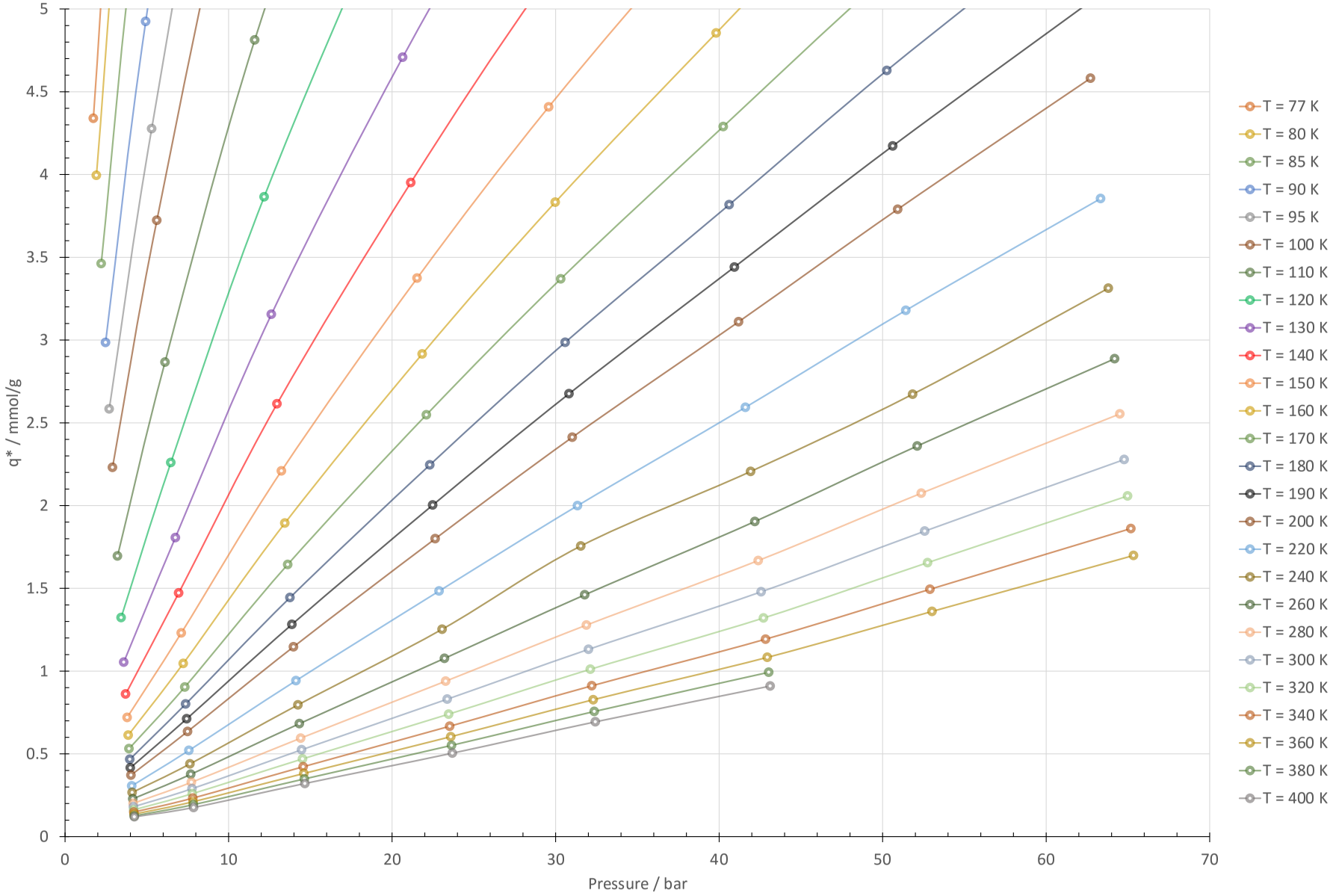

Figure 5.3: The higher temperature isotherms not discernible in figure 5.2.

Firstly, the total results exhibit the expected tendencies (see figure 2.2 for comparison): at constant temperature T, the adsorbed quantity q^* increases as the pressure P increases. At low P, q^* is proportional to P (the Henry's Law isotherm). At high T, q^* is essentially linear over the whole pressure range, as was expected.

During this process, we trialed the second experimental procedure, B, detailed in 4.6, to verify its validity and confirm our already taken results, as seen in figure 5.4. First of all, the pressure variation over a single measurement session is, due to the much smaller volume being compressed, much larger compared to our normal measurements: the variation of around 30 bar (corresponding to a factor higher than 7, from 4 bar to 35 bar) in around 30 cm^3 with a few grams of adsorbent material suggests it is a very efficient compressor.

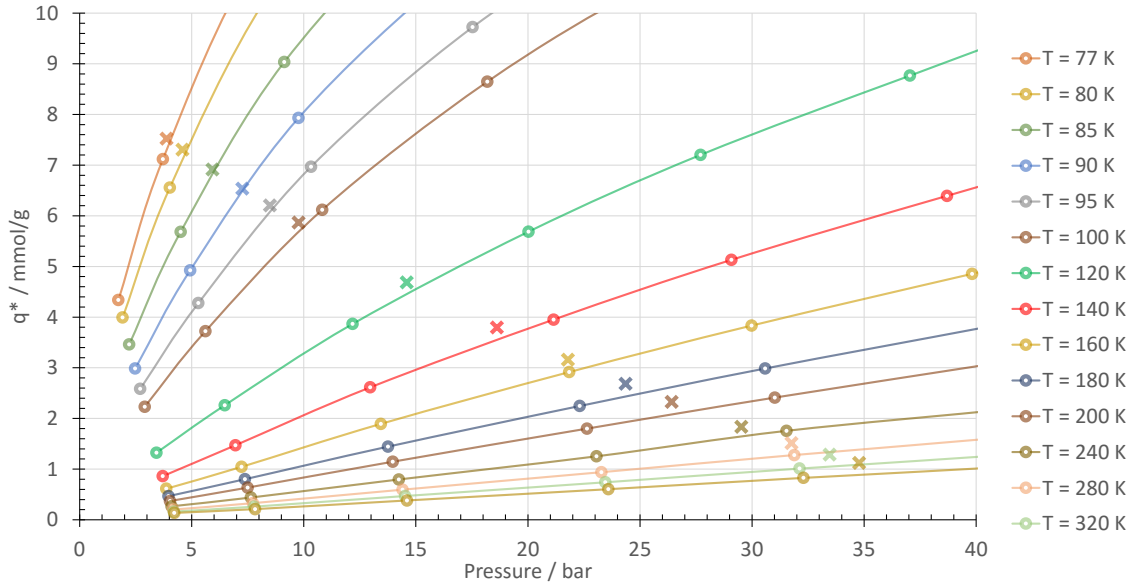

Figure 5.4: The points obtained using procedure B (crosses) overlapped with the total results from figure 5.2.

As can be seen, the points overlap with the tendency exhibited by the results in the first method and start to drift away for larger temperatures. As we had already discussed in section 4.6, this might imply an error, even if minimal, in one of the volumes of the system, V_0 or V_1, as this method is much more sensitive in that regard due to a smaller total system volume (about 15 times smaller): a 0.5 cm^3 variation induces errors up to 20% at higher temperatures, where the results drift away. Another possible explanation for this slight upwards drift is the existence of a leak, which would be more noticeable in pressure as time went on when compared to a much larger volume. A leak would lower the pressure of the system, which, as it's assumed we conserve the total quantity of neon, makes it seem like more gas is adsorbed. This explanation was discarded after extensive leak testing.

As explained in section 4.3, the results presented in figures 5.2, 5.3 and 5.4 were

only taken up to 400 K, due to an initial concern in not damaging the sample. This solder held up until the experiments above 400 K and 70 bar, where we started to have repetitive leaks in the filling, which motivated us to move on to the higher-temperature, more resistant Pb-based solder.

5.2 400 K to 500 K results

The filling and sealing of the vessel was then made with the 296 ºC Pb solder and pressure-tested at room temperature up to 40 bar for leaks, with positive results. The question was whether the sample had been damaged by the soldering temperature or not. Thus, we performed measurements to evaluate the sample's damage, which yielded the results in figure 5.5.

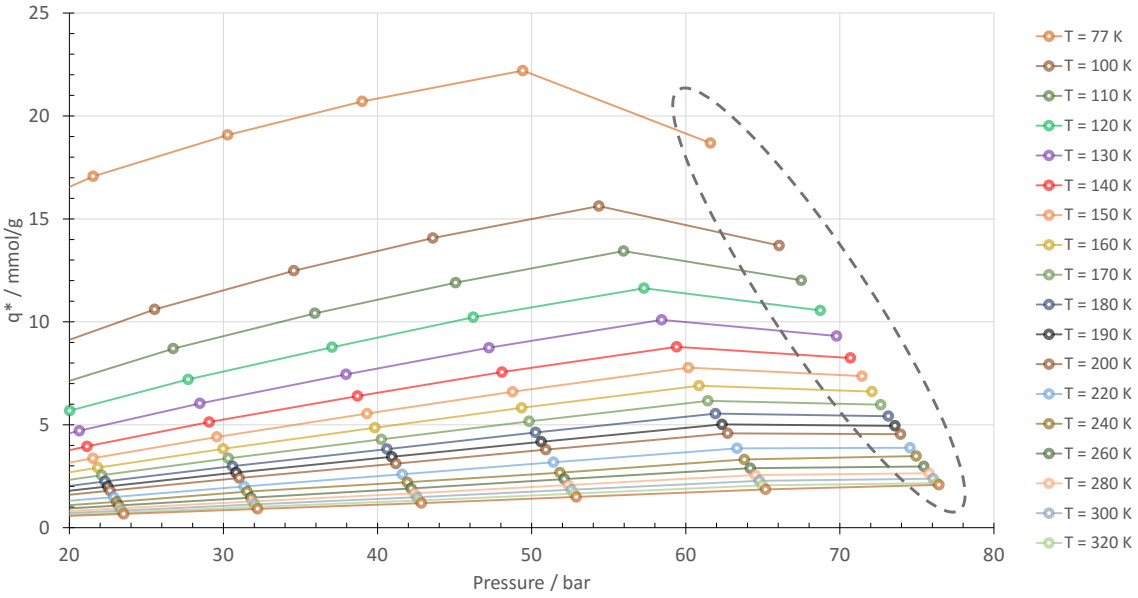

Figure 5.5: In the dashed ellipse, the points taken after the 296 ºC soldering, with the previous results.

As we can see, the sample most definitely lost adsorptive capabilities, and so we could conclude that it was damaged by the high temperature applied when soldering. A thermogravimetric analysis made by LATPE showed that decomposition of the sample can happen, in just a few minutes, anywhere above 275 ºC, compared to the 300 ºC suggested in figure 3.2. It's likely that our sample suffered such a degradation during the soldering process, which is a bit more complicated at these higher temperatures (due to the considerable heating power required).

Moreover, at around 340 K, with a pressure of 76 bar in the vessel, the screw filling opened a very small leak and consequently experiments had to be stopped. Regardless, it was shown that the sample was damaged and so any further experiments would not be performed.

5.3 Analysis

5.3.1 Error and correction analysis

The quantitative and qualitative effects of errors and the applied corrections – in volumes, adsorbent mass, considering the gas ideal, and considering no thermal expansion – in the adsorbed quantity results was an aspect analyzed throughout the measurement process. An analysis was made at the four extremes in temperature and pressure to gauge the influence of each possible error and is presented in table 5.1.

Table 5.1: The percentual effect on the adsorbed quantity q^* at the temperature and pressure extremes of measurement when given errors are made.

	Percentage error in q^* / %			
Type of error	77 K 2 bar	360 K 4 bar	77 K 50 bar	360 K 65 bar
Ideal instead of real gas	0.6	2.2	8.7	41.6
No thermal expansion	1.0	0.5	1.3	1.7
5% error in V_{vessel}	4.8	12.1	3.9	13.5
2% error in V_2	2.3	15.7	3.5	18.5
5% error in $m_{adsorbent}$	4.9	0.5	3.2	1.7

For the ideal gas approximation, at higher pressures, as the compressibility factor Z is higher, the error committed is up to 41.6% at its highest, which proves the real gas correction was mandatory. An example of the result of our correction is in figure 5.6.

The thermal expansion effect shows to be at most 2% significant, but the correction was however maintained throughout the analysis.

Despite our confidence in the volume determination, we analyzed the sensitivity of the system to an error in these determinations at several points. A 5% error in the vessel volume is an absolute error of around 0.4 cm^3, which is quite large for the observed result variance in the method of volume determination used (section 4.7). Regardless, if such an error existed, its effect would apparently be more pronounced at higher temperatures. A 2% error in the calibrated volume V_2 is an absolute error of around 3 cm^3. Similar to the error in the vessel volume, its effect would be more pronounced at higher temperatures.

The most likely source of error is the mass of the adsorbent. In this case, an error of 5% was estimated, which would be an absolute error of around 0.2 g. This is a possible error, as the vessel was activated when already mounted in the system, which made it impossible to reweigh and measure the adsorbent mass. As can be seen in figure 3.2, this can reduce the mass of adsorbent by a small amount (which seems to be approximately 5%) and the impact it can have on the results ranges from 0.5% to 4.9%.

The pressure expansion of the vessel was, as already mentioned, relatively insignificant, causing errors below 0.05% at its most, and so it's not included in this analysis or the treatment made.

5.3.2 Comparison with gravimetric data

Results from a commercial gravimetric system from our partner laboratory within the context of the project were available in the form of isotherms at 0 ºC (273 K), 30 ºC (303 K) and 70 ºC (343 K). Therefore, we could compare our isotherms at 300 K and 340 K to their isotherms at 30 ºC and 70 ºC, with a small 3 ºC difference (figure 5.6). Regardless, in this range, the variation of adsorption quantity with temperature is already quite small and thus the results at these temperatures should be quite close. Our results were in agreement with the experimental data obtained by LATPE's commercial system, having however not shown agreement with the already mentioned simulations done by Prof. J. P. Mota.

As detailed before, after applying the real gas correction (which cannot be wrong, only insignificant in certain cases) our data shifted significantly and showed agreement with the results obtained by LATPE, as can be seen in figure 5.6.

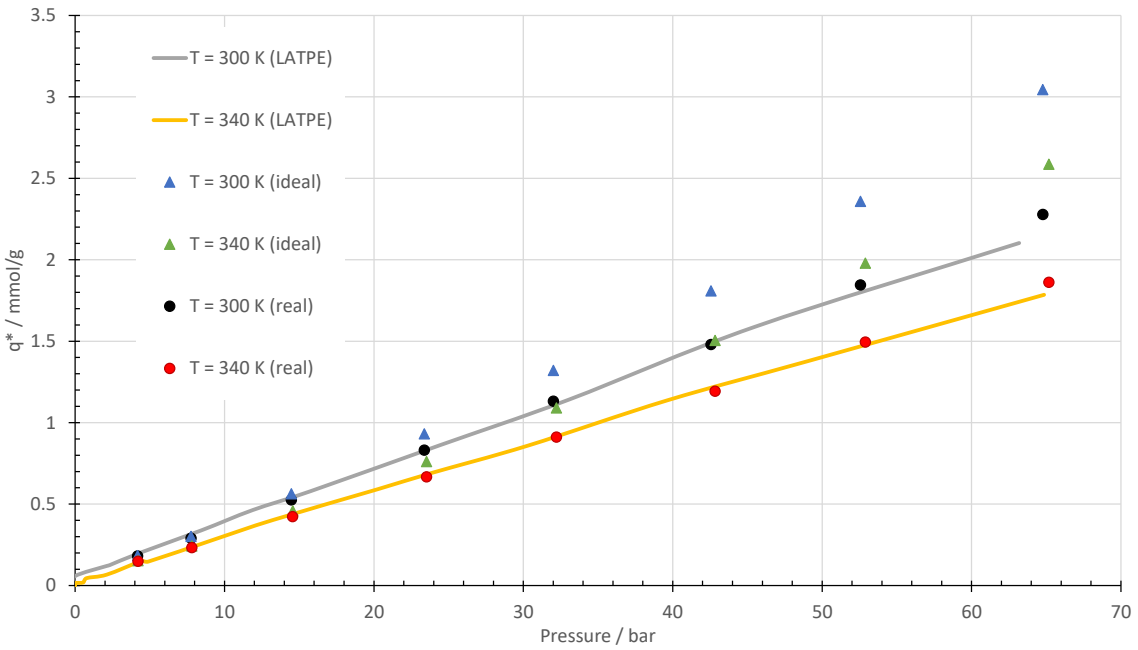

Figure 5.6: Comparison between our 300 K and 340 K (ideal and real gas) isotherms with the 303 K and 343 K isotherms from LATPE's gravimetric apparatus. The effect of the real gas correction is noticeable.

As can be seen in the above figure, the data matches quite closely on the range in which we measured, which is up to 65 bar at these temperatures, which is a very good sign to validate our measurements obtained in a completely different system and method: this agreement gives us confidence on the system built during this work.

5.3.3 Isosteric heat of adsorption

Having access to the isotherms, we can trace out isosteric (constant q^*) curves, presented in figure 5.7. These were obtained by interpolating the isotherm values in figure 5.2 and solving for given adsorbed quantities q^*. Using equation 2.5, we can calculate the adsorption heat as a function of adsorbed quantity (figure 5.8):

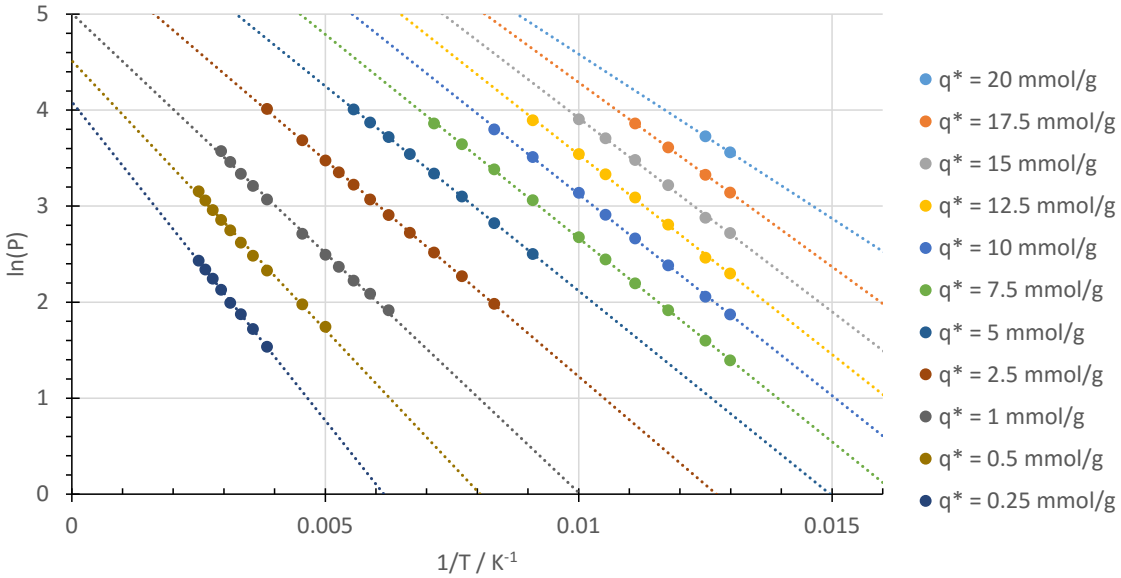

Figure 5.7: The isosthers calculated from the data of figure 5.2.

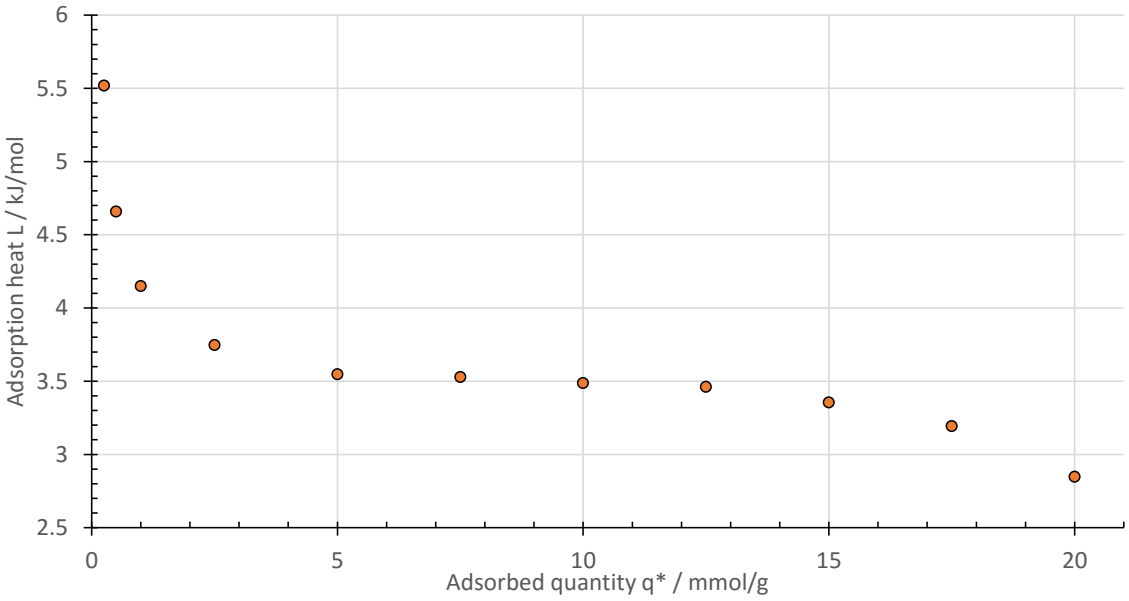

Figure 5.8: Adsorption heat vs. adsorbed quantity, through equation 2.5 and figure 5.7.

A comparison between our results and the data we had access to is presented in figure 5.9.

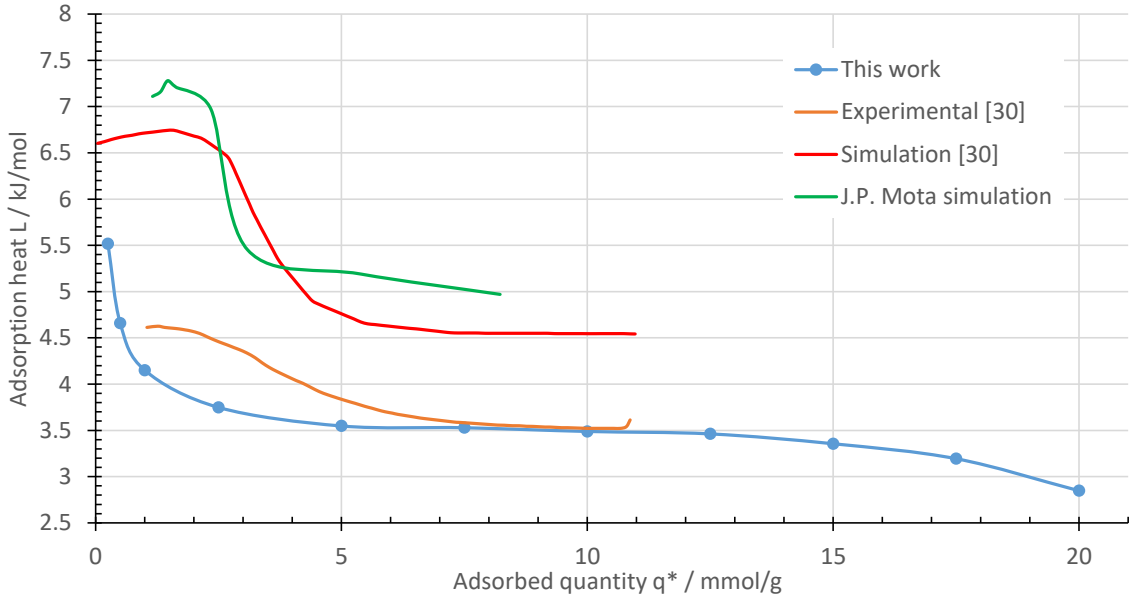

Figure 5.9: Comparison between our experimental data, the experimental and simulation data from [30], and the simulations done by Prof. J.P. Mota.

As we can see, our results agree roughly with the previous experimental results taken in 2013 [30]. The main difference lies in our rapid increase of adsorption heat for lower adsorbed quantities. It is simple in particular to notice that in fact, the adsorption heat is always much less than 20 kJ/mol (2.2.1.2), which lets us conclude that, effectively, this process was physisorption.

As it is expected, for low q^*, the occupied sites are the most energetically favorable: the heat of adsorption decreases as q^* increases. With q^* between 1 mmol/g and 15 mmol/g, the heat is relatively constant. At higher q^*, higher filling, the heat seems to decrease, indicating that all the obvious adsorption sites are occupied.

Our results, however, are significantly lower (50% to 200%) than both the simulations, as are Hulvey, Z. *et al*'s experimental results. Especially worth nothing is that the simulations also roughly agreed with each other, being around the same values with a similar tendency.

Chapter 6

Conclusions

A system for volumetric adsorption measurements in the 77 K to 400 K and 0 bar to 80 bar range was developed: an adsorption vessel, a calibrated volume and a gas manifold were dimensioned, built, and tested.

In specific, the development of a cooling and heating system to properly control the vessel's temperature was an interesting challenge in which we succeeded: the initial idea was to do the measurements up to room temperature in one of the laboratory's cryocoolers, with the upper range done from room temperature without a cryocooler, or, at least, forcing a thermal decoupling of the measurement cell from the cold finger: for this temperature range, the developed system is functional and performed a full set of measurements in a practical manner. Let us note that this is the first time that such a system was developed and that measurements up to 200 ºC were obtained in the Laboratory of Cryogenics!

Also worth mentioning are the several setbacks caused by the vessel's screw solder filling. The vessel and solder set failed to accommodate pressures larger than 75 bar, having often leaked in this range. This hindered and limited our measurements as it implied redoing the screw soldering, remounting the heating and thermometer resistors and reactivating the sample every time it happened. On a time constraint as this work was, this was often relatively time-consuming. Possible reasons for this constant solder failure at higher pressures and temperatures are aplenty: the solder had vulnerabilities caused by a higher temperature (most, if not all, of these failures occurred at higher temperatures), the copper dilatation due to pressure fractured the solder filling, or the solder simply didn't hold up in those pressures when applied in that amount. Again, this would require lengthier tests on the viability of this option. The use of a disposable vessel, as we initially attempted to avoid, has to be eventually reconsidered if these tests fail.

Despite these problems, we succeeded to make a relatively extensive study of neon

adsorption on HKUST-1 in quite a large temperature and pressure range. It is proved positive in the sense that the results we obtained through our method matched the results obtained by LATPE through a commercial gravimetric setup. The results on adsorption heat also matched experimental data taken by other groups, which again proved positive. However, in the scope of the project and comparing to the previously made simulations, the material proved less suitable than initially expected: its temperature tolerance seemed to be smaller than expected, as it started to decompose at around 300 ºC, which in the case of our 296 ºC Pb solder proved prohibitive even in short amounts of time, as the soldering is done with the sample inside the vessel. We were able to verify this with the results taken, which showed substantially lowered adsorption capabilities.

There are improvements to be done other than the study on the viability of the solder screw filling, which is the most significant one in order to fulfill the initial requirements (up to 100 bar, 77 K to 500 K). Some change of the insulation used in the cooling and heating system might be needed, as the initial part of the heating ramp (from 77 K to around 95 K: see figure 4.17, for instance) is long and slightly unstable at times due to liquid nitrogen contact with the vessel: this might be due to some form of leak in the insulation, and destabilizes the controller due to its unpredictability. Another noteworthy improvement to be had is the research and use of a better packing method. The figures of 42% and 45% obtained for the packing factor ϵ were farther than expected from the ideal 36%. Yet another improvement is in the activation procedure, which doesn't allow for the measurement of the post-activation adsorbent mass as it involves disconnection of the vessel from the system, leading to an influx of unwanted air and "deactivating" the sample, which would require another activation and again we would have no knowledge of the final adsorbent mass.

In the context of the project, some work on more promising, non-commercial adsorbent samples is to be done, which, with the system that is currently mounted, is achievable with trustworthy results.

References

[1] J. Burger, H. Holland, M. Ter Brake, G. Venhorst, E. Hondebrin, R. J. Meier, H. Rogalla, R. Coesel, W. Dierssen, R. Grim, D. Lozano-Castello, and A. Sirbi, "Vibration-free 5 K sorption cooler for ESA's Darwin mission", *European Space Agency, (Special Publication) ESA SP*, vol. 42, no. 539, pp. 379–384, 2003. DOI: 10.1016/S0011-2275(02)00008-5.

[2] European Space Agency, "Statement of Work for "Development of a 40-80 K vibration-free cooler"", 2014.

[3] A. N. Shmroukh, A. H. H. Ali, and S. Ookawara, "Adsorption working pairs for adsorption cooling chillers: A review based on adsorption capacity and environmental impact", *Renewable and Sustainable Energy Reviews*, vol. 50, pp. 445–456, 2015. DOI: 10.1016/j.rser.2015.05.035.

[4] L. W. Wang, R. Z. Wang, and R. G. Oliveira, "A review on adsorption working pairs for refrigeration", *Renewable and Sustainable Energy Reviews*, vol. 13, no. 3, pp. 518–534, 2009. DOI: 10.1016/j.rser.2007.12.002.

[5] J. U. Keller and R. Staudt, *Gas adsorption equilibria: Experimental methods and adsorptive isotherms*, September 2013. Springer, 2005, vol. 1, pp. 1–422. DOI: 10.1007/b102056.

[6] J. W. Gibbs, "A Method of Geometrical Representation of the Thermodynamic Properties of Substances by Means of Surfaces", *Transactions of the Connecticut Academy of Arts and Sciences*, vol. 2, pp. 382–404, 1873.

[7] J. M. Thomas, "The existence of endothermic adsorption", *Journal of Chemical Education*, vol. 38, no. 3, pp. 138–139, 1961. DOI: 10.1021/ed038p138.

[8] R. Krishna and J. M. Van Baten, "Hydrogen bonding effects in adsorption of water-alcohol mixtures in zeolites and the consequences for the characteristics of the Maxwell-Stefan diffusivities", *Langmuir*, vol. 26, no. 13, pp. 10 854–10 867, 2010. DOI: 10.1021/la100737c.

[9] M. Monthioux, E. Flahaut, C. Laurent, W. Escoffier, B. Raquet, W. Bacsa, P. Puech, B. Machado, and P. Serp, "Properties of Carbon Nanotubes", in *Handbook of Nanomaterial Properties*, Springer, 2014, ch. 1, p. 29. DOI: 10.1007/978-3-642-31107-9.

[10] K. Y. Foo and B. H. Hameed, "Insights into the modeling of adsorption isotherm systems", *Chemical Engineering Journal*, vol. 156, no. 1, pp. 2–10, 2010. DOI: 10.1016/j.cej.2009.09.013.

[11] S. Brunauer, P. H. Emmett, and E. Teller, "Adsorption of Gases in Multimolecular Layers", *Journal of the American Chemical Society*, vol. 60, no. 1, pp. 309–319, 1938. DOI: 10.1021/ja01269a023.

[12] P Kisliuk, "The Sticking Probabilities of Gases Chemisorbed on the Surfaces of Solids", *Journal of Physics and Chemistry of Solids*, vol. 3, pp. 95–101, 1957. DOI: 10.1016/0022-3697(58)90132-X.

[13] Y. A. Çengel and M. A. Boles, "The Clapeyron Equation", in *Thermodynamics: An Engineering Approach*, 5th ed., Boston, MA: McGraw-Hill, 2002, ch. 12, pp. 658–660, ISBN: 9780072884951.

[14] *Cocarb Solution Activated Carbon*. [Online]. Available: http://www.cocarb.com/products/activated-carbon/ (visited on 07/18/2016).

[15] *Coldstream Outdoor Zeolite*. [Online]. Available: http://www.coldstreamindustries.com/zeolite/5-lb-zeolite-pure-97.html (visited on 07/18/2016).

[16] M. Breitbach, D. Bathen, and H. Schmidt-Traub, "Effect of Ultrasound on Adsorption and Desorption Processes", *Industrial & Engineering Chemistry Research*, vol. 42, no. 22, pp. 5635–5646, 2003. DOI: 10.1021/ie030333f.

[17] R. Berenguer, J. P. Marco-Lozar, C. Quijada, D. Cazorla-Amorós, and E. Morallón, "Electrochemical regeneration and porosity recovery of phenol-saturated granular activated carbon in an alkaline medium", *Carbon*, vol. 48, no. 10, pp. 2734–2745, 2010. DOI: 10.1016/j.carbon.2010.03.071.

[18] K. Y. Foo and B. H. Hameed, "Microwave-assisted regeneration of activated carbon", *Bioresource Technology*, vol. 119, pp. 41–47, 2012. DOI: 10.1016/j.biortech.2012.05.061.

[19] N. Lamia, M. Jorge, M. A. Granato, F. A. Almeida Paz, H. Chevreau, and A. E. Rodrigues, "Adsorption of propane, propylene and isobutane on a metal-organic framework: Molecular simulation and experiment", *Chemical Engineering Science*, vol. 64, no. 14, pp. 3246–3259, 2009. DOI: 10.1016/j.ces.2009.04.010.

[20] N. Greeves, *ChemTube3D*, 2015. [Online]. Available: http://www.chemtube3d.com/solidstate/MOF-HKUST-1.html (visited on 07/18/2016).

[21] J. P. Mota, *Private communication*, 2016.

[22] G. F. M. Wiegerinck, J. F. Burger, H. J. Holland, E. Hondebrink, H. J. M. Ter Brake, and H. Rogalla, "A sorption compressor with a single sorber bed for use with a Linde-Hampson cold stage", *Cryogenics*, vol. 46, no. 1, pp. 9–20, 2006. DOI: 10.1016/j.cryogenics.2005.08.006.

[23] D. Doornink, J. Burger, and H. ter Brake, "Sorption cooling: A valid extension to passive cooling", *Cryogenics*, vol. 48, no. 5-6, pp. 274–279, 2008. DOI: 10.1016/j.cryogenics.2008.03.012.

[24] A. S. Technologies and FCT-UNL, "Proposal for "Development of a 40 K - 80 K vibration free cryocooler"", Tech. Rep., 2014.

[25] P. D. Bentley, "The modern cryopump", *Vacuum*, vol. 30, no. 4-5, pp. 145–158, 1980. DOI: 10.1016/S0042-207X(80)80677-4.

[26] I. Catarino, G. Bonfait, and L. Duband, "Neon gas-gap heat switch", *Cryogenics*, vol. 48, no. 1-2, pp. 17–25, 2008. DOI: 10.1016/j.cryogenics.2007.09.002.

[27] C. K. Chan, E. Tward, and K. I. Boudaie, "Adsorption isotherms and heats of adsorption of hydrogen, neon and nitrogen on activated charcoal", *Cryogenics*, vol. 24, no. 9, pp. 451–459, 1984. DOI: 10.1016/0011-2275(84)90001-8.

[28] J. Moellmer, A. Moeller, F. Dreisbach, R. Glaeser, and R. Staudt, "High pressure adsorption of hydrogen, nitrogen, carbon dioxide and methane on the metal-organic framework HKUST-1", *Microporous and Mesoporous Materials*, vol. 138, no. 1-3, pp. 140–148, 2011. DOI: 10.1016/j.micromeso.2010.09.013.

[29] I. Senkovska and S. Kaskel, "High pressure methane adsorption in the metal-organic frameworks Cu3(btc)2, Zn2(bdc)2dabco, and Cr3F(H2O)2O(bdc)3", *Microporous and Mesoporous Materials*, vol. 112, no. 1-3, pp. 108–115, 2008. DOI: 10.1016/j.micromeso.2007.09.016.

[30] Z. Hulvey, K. V. Lawler, Z. Qiao, J. Zhou, D. Fairen-Jimenez, R. Q. Snurr, S. V. Ushakov, A. Navrotsky, C. M. Brown, and P. M. Forster, "Noble gas adsorption in copper trimesate, HKUST-1: An experimental and computational study", *Journal of Physical Chemistry C*, vol. 117, no. 39, pp. 20 116–20 126, 2013. DOI: 10.1021/jp408034u.

[31] F. Raganati, V. Gargiulo, P. Ammendola, M. Alfe, and R. Chirone, "CO2 capture performance of HKUST-1 in a sound assisted fluidized bed", *Chemical Engineering Journal*, vol. 239, pp. 75–86, 2014. DOI: 10.1016/j.cej.2013.11.005.

[32] P. I. O'Toole and T. S. Hudson, "New high-density packings of similarly sized binary spheres", *Journal of Physical Chemistry C*, vol. 115, no. 39, pp. 19 037–19 040, 2011. DOI: 10.1021/jp206115p.

[33] C. Song, P. Wang, and H. A. Makse, "A phase diagram for jammed matter",*Nature*, vol. 453, no. 7195, pp. 629–632, 2008. DOI: 10.1038/nature06981.

[34] M Suzuki, *Fundamentals of Adsorption*. 1993, p. 798, ISBN: 0080887724. [Online]. Available: https://books.google.com/books?id=fOmiFuCCBJwC.

[35] J. Case, L. Chilver, and C. T. Ross, "Thin shells under internal pressure", in *Strength of Materials and Structures*, Butterworth-Heinemann, 1999, ch. 6, pp. 152–168. DOI: 10.1016/B978-034071920-6/50010-8.

[36] D. Martins, "40 K Neon Liquid Energy Storage Unit", PhD thesis, Universidade Nova de Lisboa, 2014, p. 54.

[37] G. Tomás, "Medidas da condutividade térmica duma espuma de cobre a baixa temperatura", Master's thesis, Universidade Nova de Lisboa, FCT-UNL, 2014.

[38] E. Lemmon, M. L. Huber, and M. O. McLinden, *NIST Standard Reference Database 23: Reference Fluid Thermodynamic and Transport Properties, version 9.1*, Gaithersburg, 2013.

[39] *Material Properties: OFHC Copper*, 2010. [Online]. Available: http://cryogenics.nist.gov/MPropsMAY/OFHCCopper/OFHC_Copper_rev.htm (visited on 07/12/2016).

Appendix A

Technical drawings

In this appendix there are the main technical drawings made in the whole development process, from testing to the final components of the system.

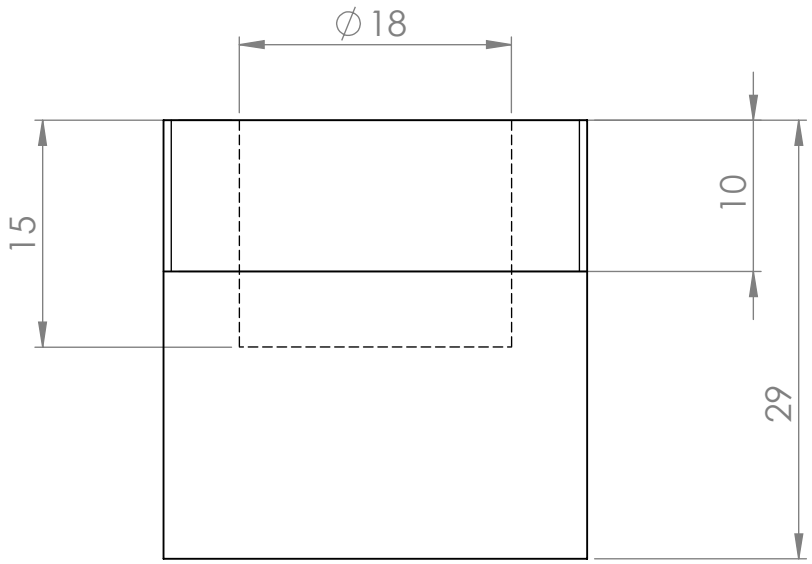

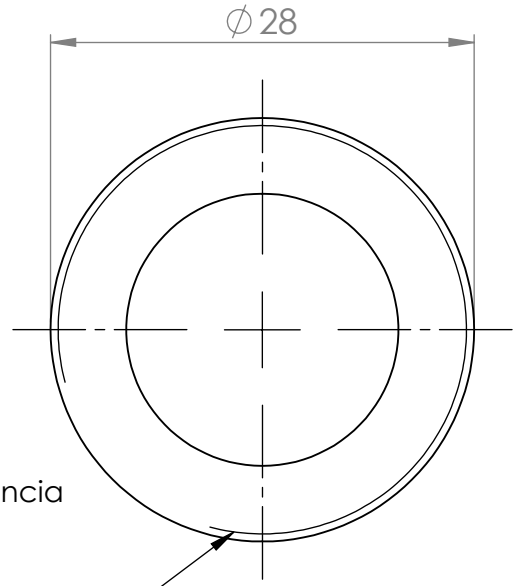

Rosca sobre toda a circunferência
(erro do Solidworks)
Passo: 1mm
Comprimento: 10mm
(pelo menos, para "cap" bater)

	NAME		DATE		
DRAWN	Mário Xavier		21/01/16		
CHK'D	Grégoire Bonfait		21/01/16		

TITLE:

Adsorption Cell Test

MATERIAL: Copper

Laboratório Criogenia

A4

SCALE:2:1

SHEET 1 OF 1

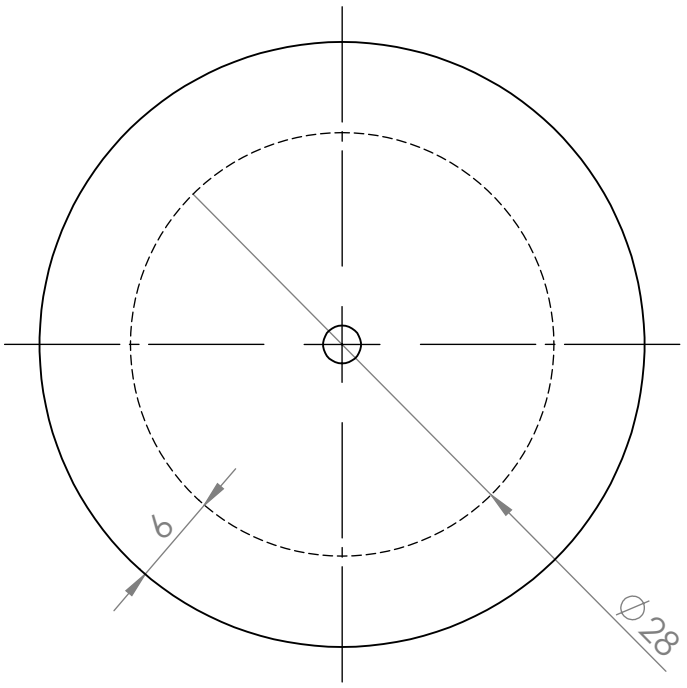

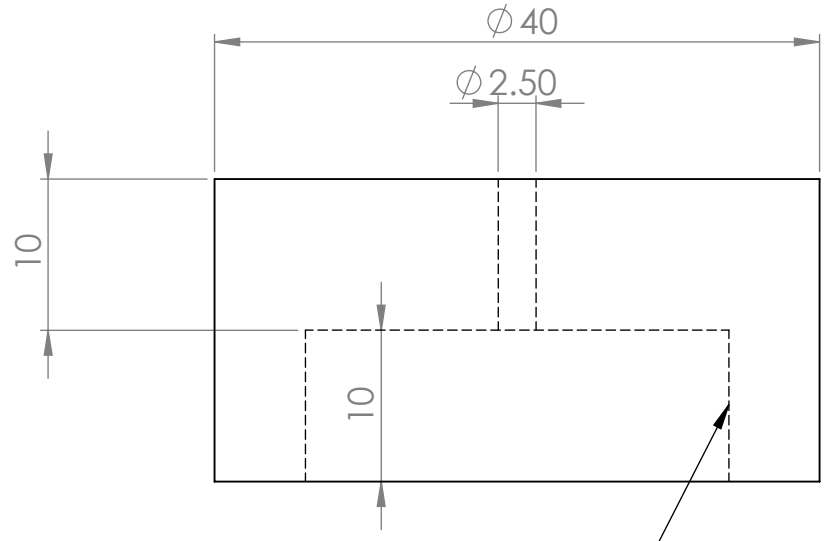

Rosca complementar à adsorption cell:
Passo: 1mm
Comprimento: 10mm
O "cap" deve bater no topo da célula

	NAME	SIGNATURE	DATE
DRAWN	Mário Xavier		22/01/16
CHK'D	Grégoire Bonfait		22/01/16

TITLE: Screw Cap Test

MATERIAL: Copper

Laboratório Criogenia

A4

SCALE:2:1

SHEET 1 OF 1

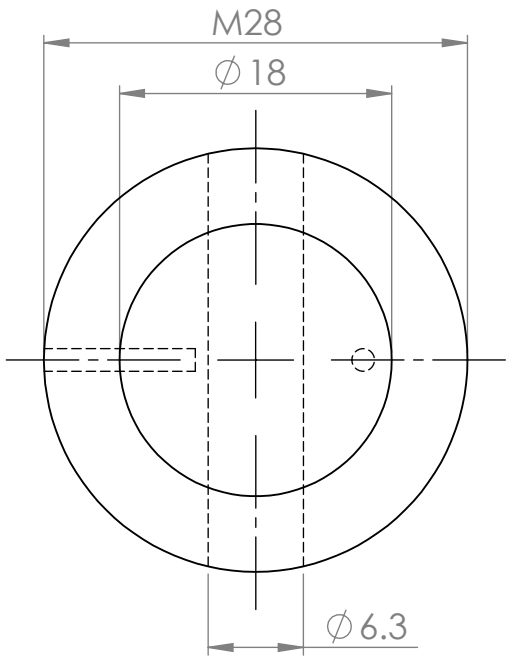

Rosca M28 a partir do topo
Passo: 1mm
Comprimento: suficiente para o topo da célula "bater" no cap (pelo menos 10 mm)

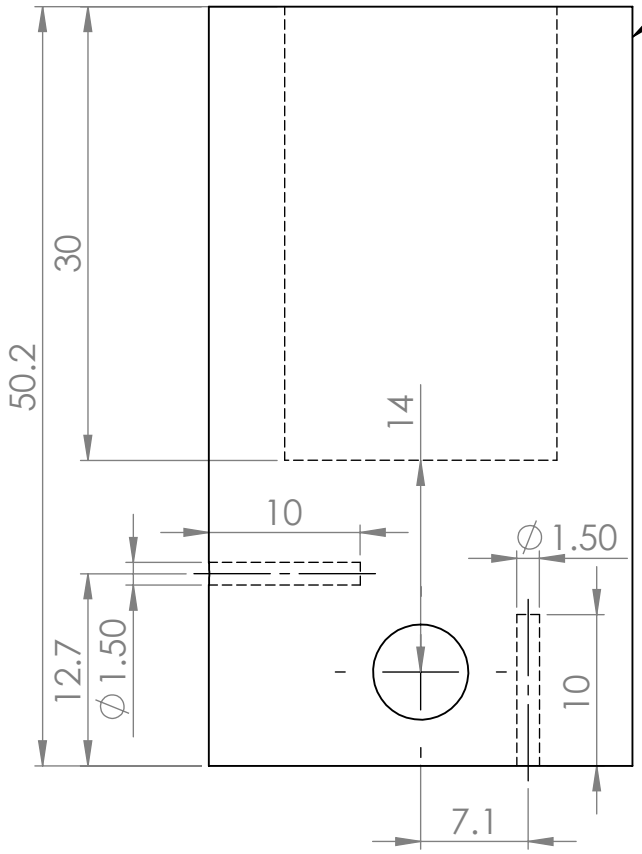

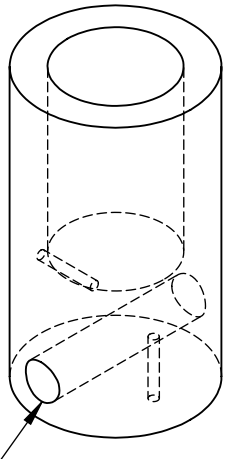

1/4 polegada
Para heater cartridge.
Entrar "à justa"

	Nome	Data
Desenho	MX	04/04/16
Verificação	GB	04/04/16

Peça:

Célula de adsorção p/ altas pressões

Lab. Criogenia FCT-UNL

MATERIAL: Cobre

1 peça

Tamanho: A4

Escala: 2 : 1

Tolerância: X: ±0.1

Nome desenho: Cu_Adsorption_Cell

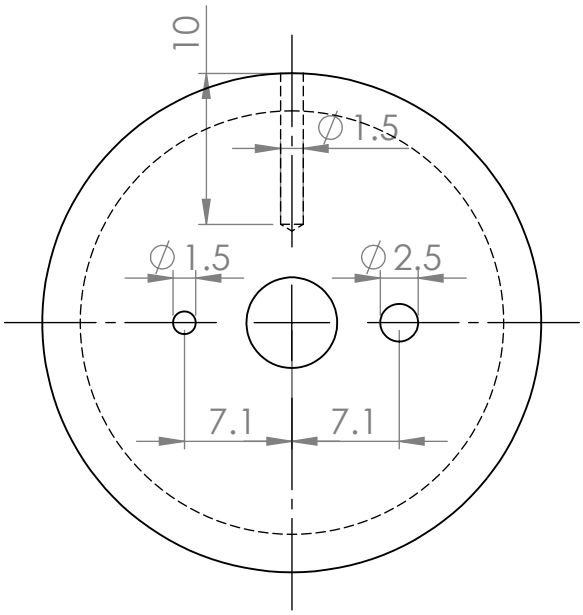

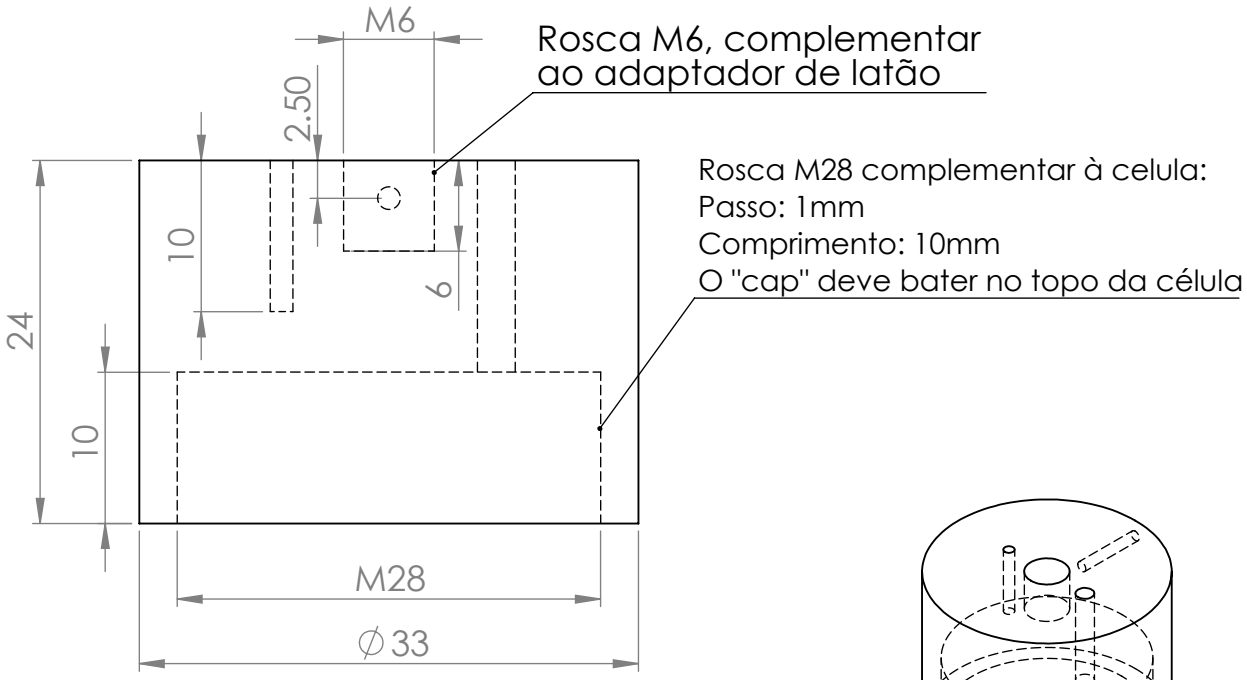

	Nome	Data
Desenho	MX	04/04/16
Verificação	GB	04/04/16

Peça:

Cap da célula
de adsorção p/ altas pressões

Lab. Criogenia FCT-UNL

MATERIAL:
Cobre

1 peça

Tamanho: A4

Escala: 2 : 1

Tolerância:
X: ±0.1

Nome desenho:
Cu_Adsorption_Cell

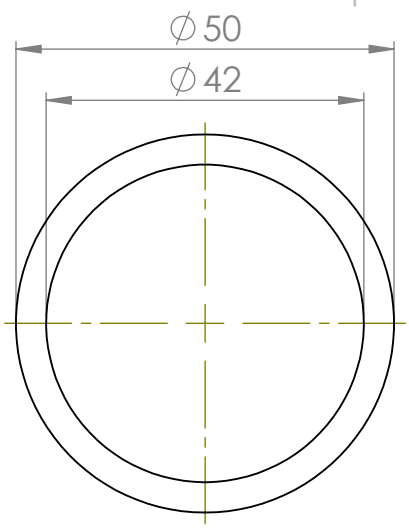

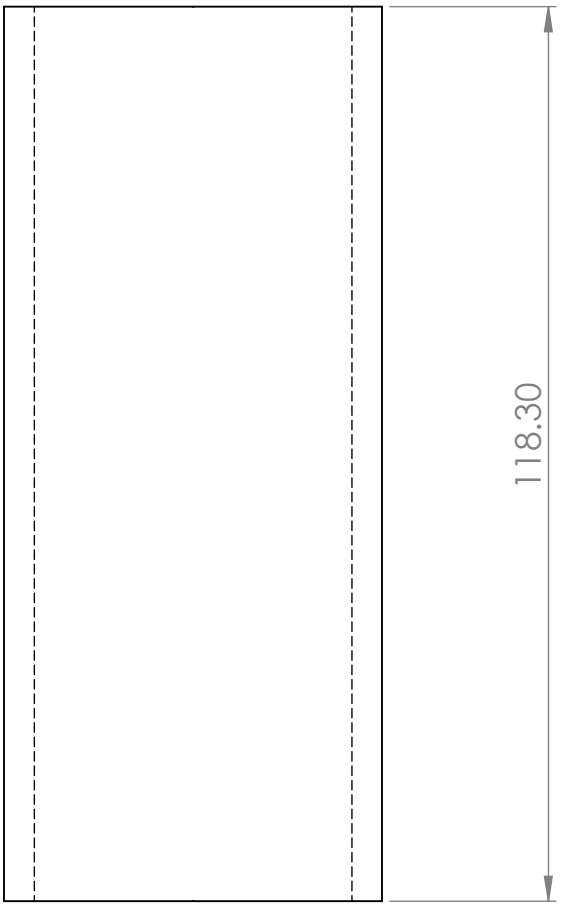

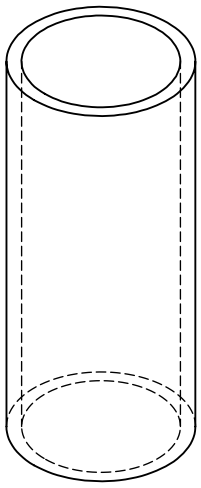

	Nome	Data
Desenho	MX	15/04/16
Verificação	GB	15/04/16

Peça:

Volume calibrado p/ altas pressões

Lab. Criogenia FCT-UNL

MATERIAL: Inox

1 peça

Tamanho: A4

Escala: 1 : 1

Tolerância: X: ±0.1

Nome desenho: SS_Calibrated_Volume

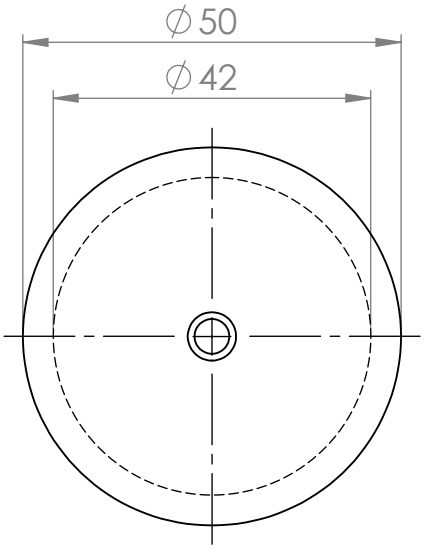

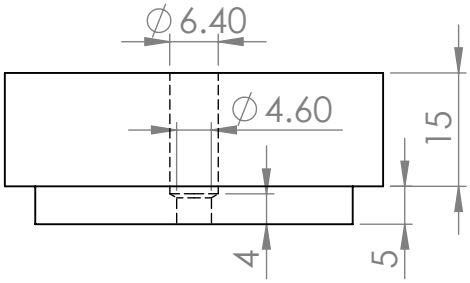

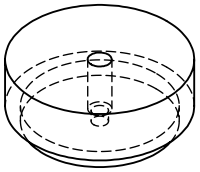

	Nome	Data
Desenho	MX	18/04/16
Verificação	GB	19/04/16

MATERIAL: Inox

Peça: **Cap superior do volume calibrado p/ altas pressões**

Lab. Criogenia FCT-UNL

1 peça

Tamanho: A4

Escala: 1 : 1

Tolerância: X: ±0.1

Nome desenho: SS_Calibrated_Volume_Cap_Top

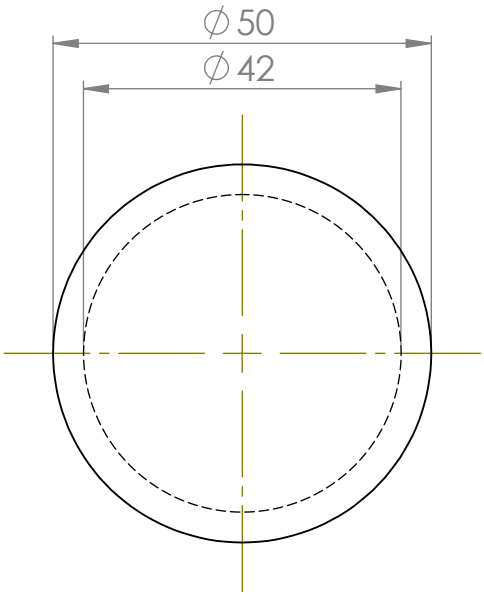

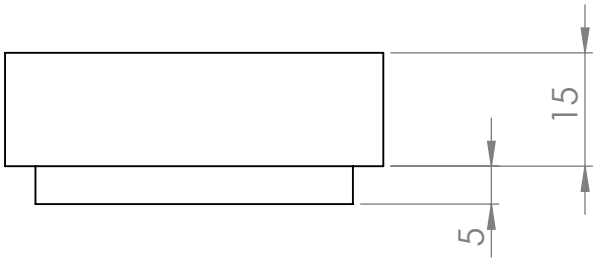

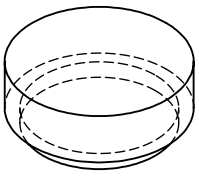

	Nome	Data
Desenho	MX	18/04/16
Verificação	GB	19/04/16

MATERIAL: Inox

Tamanho: A4

Escala: 1 : 1

Tolerância: X: ±0.1

Peça:

Cap inferior do volume calibrado p/ altas pressões

Nome desenho: SS_Calibrated_Volume_Cap

Lab. Criogenia FCT-UNL

1 peça